DISSOLUTION MORPHOLOGY OF LITHIUM FLUORIDE SURFACES

ELECTRON MICROSCOPIC STUDY

OF

DISSOLUTION MORPHOLOGY

OF

LITHIUM FLUORIDE SURFACES

By

T. R. RAMACHANDRAN, B.Sc. (Hons.), B.E. (Met.)

A Thesis

Submitted to the Faculty of Graduate Studies

in Partial Fulfilment of the Requirements

for the Degree

Master of Science

McMaster University

October 1965

MASTER OF SCIENCE (1965)
(Metallurgy)

McMASTER UNIVERSITY
Hamilton, Ontario.

TITLE: Electron Microscopic Study of Dissolution Morphology of Lithium Fluoride Surfaces

AUTHOR: T. R. Ramachandran, B.Sc. (Hons.) (Sri Venkateswara)

B.E. (Met.) (Indian Institute of Science)

SUPERVISOR: Professor M. B. Ives

NUMBER OF PAGES: ix, 100

SCOPE AND CONTENTS: The dislocation etch pits formed on the cleavage surfaces of lithium fluoride in an aqueous solution containing varying concentrations of ferric ions are investigated by electron microscopy. The results obtained reveal the powerful influence of the inhibitor in the stabilisation of kinks and macroledges. There is some evidence for the nucleation of dissolution at imperfections other than the dislocations. Dissolution spirals are observed in some cases suggesting the presence of helical dislocations in lithium fluoride.

ACKNOWLEDGEMENTS

The author wishes to thank Professor M. B. Ives for his constant encouragement, advice and aid throughout the course of this work, without which this project could not have been completed.

Thanks are extended to Professor R. K. Ham and Professor G. R. Purdy for helpful discussions. Valuable assistance was provided by Mr. H. Walker and Mrs. M. S. Baskin in the early stages of the experimental work.

The author wishes to acknowledge the receipt of a McMaster Graduate Scholarship and the aid of a research grant from the United States Office of Naval Research.

TABLE OF CONTENTS

LIST OF FIGURES

Platinum-carbon replicas of lithium fluoride surfaces etched with:

16. 0.3 p.p.m. Fe, instantaneous etch.
17. 0.3 p.p.m. Fe, 30 second etch.
18. 1.5 p.p.m. Fe, instantaneous etch.
19. 1.5 p.p.m. Fe, 30 second etch.
20. 6 p.p.m. Fe, instantaneous etch.
21. 6 p.p.m. Fe, 30 second etch.
22. 15 p.p.m. Fe, instantaneous etch.
23. 15 p.p.m. Fe, 30 second etch.
24. 30 p.p.m. Fe, instantaneous etch.
25. 30 p.p.m. Fe, 30 second etch.
26. 60 p.p.m. Fe, instantaneous etch.
27. 60 p.p.m. Fe, 30 second etch.
28. 150 p.p.m. Fe, instantaneous etch.
29. 150 p.p.m. Fe, 30 second etch.
30. 1.5 p.p.m. Fe, 2 minute etch.
31. 1.5 p.p.m. Fe, 2 minute etch.
32. 3 p.p.m. Fe, 30 second etch.
33. 3 p.p.m. Fe, 30 second etch.
34. 9 p.p.m. Fe, 30 second etch.
35. 9 p.p.m. Fe, 2 minute etch.
36. 9 p.p.m. Fe, 5 second etch.
37. 0.3 p.p.m. Fe, 2 minute etch.
38. 9 p.p.m. Fe, 2 minute etch.
39. 6 p.p.m. Fe, 30 second etch

INTRODUCTION

The field of crystal growth and dissolution has received a great deal of attention from various investigators in the field of physics, chemistry and metallurgy. These studies have enabled us to understand the process of dissolution based on the atomic structure of a crystal surface rather than depending on any macroscopic phenomenological concepts. Of particular interest in the studies on dissolution is the profound changes brought about by the addition of extremely small quantities of inhibitors.

The use of inhibitors in corrosive systems is, of course, not a new concept. Metallurgists have used etches to reveal the structure of metals and alloys for centuries and these, although prepared by cookbook and trial and error methods, almost invariably include a quantity of some ingredient in the etch other than the solvent. The research into the dissolution process in ionic crystals and metals has provided a basis for the development of these etchants in a more scientific manner. Most of the studies have been carried out on single crystals of high purity alkali halides, since reproducible surfaces of these materials are readily obtained by cleavage. In addition, the etchant compositions required are very simple and this has considerably aided the analysis. It is hoped that some of the mechanisms applicable to alkali halide inhibition may find application to the more important metals and alloys at a future date.

One of the important applications of the phenomenon of crystal dissolution is the development of etchants which attack preferentially the sites where imperfections in the crystal, like dislocations, vacancies

and impurity atoms, end. The etch pit method has gained considerable importance in the study of the movement of dislocations. It has the unique advantage of being applicable to quantitative measurements of dislocation velocities. The studies on etch pits have been used to advantage to find out how dislocations multiply in crystals; they have considerably helped in the understanding of the process of fracture.

There are two basic theoretical approaches to the problem of dissolution; the mechanistic theory of Burton, Cabrera and Frank, and the topographical theory of Frank. Some of the salient features of these theories will be outlined in this thesis.

The inhibited dissolution of lithium fluoride in water in the presence of iron forms the basis for this study. Electron microscopic examination of the dissolved surfaces has been carried out to study the ledges in the pit, in an attempt to understand the function of the inhibitor in the dissolution process.

CHAPTER I

SURFACE STRUCTURE AND DISSOLUTION

Topography:

The first geometric concepts of crystal surfaces were based on Platonic idealised models; in other words they represented what the surfaces ought to be rather than what they really are. The interpretation of crystal shapes in terms of space lattices of atoms has existed for a long time. The discovery of x-ray diffraction by Freidrich, Knipping and Laue showed the space lattice theory to be an inaccurate though a very valuable approximation. The first approaches to the interpretation of a surface were sought from thermodynamics and the necessary theoretical apparatus was provided by Gibbs (1) in his study of heterogeneous equilibrium. He provided a clear definition of surface energy, by which the concept of surface tension is made applicable to solids as well as liquids. He appreciated that an anisotropic surface free energy implied a non-spherical equilibrium shape, which could be thermodynamically defined as the shape which minimised the total surface energy. This approach was particularly developed by Wulff (2) who enunciated (without proving) the theorem which bears his name, providing a construction for deriving the equilibrium shape from the polar diagram of surface free energy - if a body is in its equilibrium shape, there exists a point whose perpendicular distance from every face is proportional to the surface free energy of that face.

The anisotropy of surface free energy led to the characterisation,

proposed by Frank (3) and Cabrera (4) of surfaces as:

(a) singular surfaces, corresponding to a cusped minimum in Wulff's plot giving the surface free energy as a function of orientation, and usually corresponding to a low-index plane,

(b) vicinal surfaces with orientations near those of a singular surface and formed of low-index facets separated by monomolecular ledges or steps, and

(c) non-singular or diffused surfaces whose interfacial free energy is roughly independent of orientation.

Kossel (5) and Stranski (6) introduced the fundamental premises used to develop the currently accepted geometric model for vicinal crystalline surfaces as shown schematically in Figure 1. The surface is made up of an array of low-index planes separated by ledges of monomolecular height. The ledges consist of segments lying in close-packed directions separated by kinks of monomolecular offset. The terrace-ledge-kink model of a surface has been extensively used in the areas of crystal growth, evaporation and dissolution.

Crystal dissolution and etch pit formation:

The theoretical analyses of crystal dissolution that are most widely accepted today can be grouped into two categories:

(a) those which invoke a mechanistic approach as first rigorously applied by Burton, Cabrera and Frank (7), and

(b) those based on phenomenological or kinetic arguments such as the topographical theory of Frank (8), Cabrera and Vermilyea (9) and Chernov (10). Both the treatments are based on the Kossel (5) and Stranski (6) model of a surface composed of close-packed planes separated by monatomic ledges

containing kinks. Frenkel (11), and Burton and Cabrera (12) have shown that the steps will contain a high concentration of kinks; for example, in a close-packed step in a (111) face of a face-centred cubic crystal, the mean distance between kinks is about four times the interatomic distance (7).

When a crystal dissolves, material is lost preferentially from the kinks, where binding is the weakest, thereby effecting the motion of the kinks along the ledges. By travelling the length of a ledge, a kink can produce an overall motion of that ledge by an amount equal to the offset of the kink. The localised dissolution rate will be proportional to the product of the ledge velocity (v) and the concentration of ledges (k) in the given vicinity. The theoretical analysis of the dissolution process then involves an interpretation of the dependence of v on k. The mechanistic approach differs from the topographical approach in that in the former Burton et al. (7) invoked the ledge model of dissolution and derived v as equal to $v(k)$, whereas in the latter Frank assumed a form for $v(k)$ and then developed a theory.

Mechanistic theory:

The basic concepts of the mechanistic approach to the theory of dissolution, as developed by Burton et al. (7), have been modified by Cabrera and Levine (13) and Hirth and Pound (14,15) to include a more general spectrum of materials and conditions.

As pointed out earlier, Frenkel (11), and Burton et al. (7) have shown that at temperatures of practical interest a high concentration of kinks will form along existing steps by thermal fluctuations. The latter investigators have also indicated that surface steps do not form with comparable ease and a

perfect crystal surface in equilibrium with its vapour or solution will remain essentially flat at temperatures below the melting point. The availability of surface steps may, therefore, present a problem during dissolution.

When a receding step reaches the edge of a crystal during dissolution, it is eliminated. However, a step that terminates at a screw dislocation cannot be eliminated during dissolution and such dislocations provide a constant source of steps. The edges of a crystal can also act as a source of steps during dissolution. Hirth and Pound (15) have studied the role of crystal edges during evaporation and they have calculated the evaporation coefficient of a large perfect crystal in which the edges are the only source of steps. The effects of surface imperfections like pores and cracks, dislocations, etc., on the evaporation coefficient of the crystal have also been considered (15).

On a perfect region of a crystal that is far away from surface imperfections or crystal edges, steps can be formed only by two-dimensional nucleation and this can occur only at high undersaturations. The formation of pits at dislocations will be favoured if two-dimensional nucleation can occur more readily at a dislocation than elsewhere on a surface.

The two possibilities for the formation of dislocation etch pits are:

(a) by rapid two-dimensional nucleation at a dislocation, and

(b) by removing atoms from the step that terminates at a screw dislocation.

Two-dimensional nucleation on a perfect surface:

The free energy for formation of a two-dimensional nucleus consists of a volume and a surface energy term

$$G = \frac{\pi r^2 h}{\Omega} \Delta\mu_o + 2\pi rh.\gamma \qquad \text{(i)}$$

when r and h are the radius and depth of the nucleus, γ is the surface energy, Ω the atomic volume, and $\Delta\mu_o$ the change in chemical potential when a molecule of the crystal goes into solution.

$$\Delta\mu_o = kT \ln \frac{c}{c_o} \qquad \text{(ii)}$$

where k is the Boltzmann constant, T the temperature, c_o the equilibrium concentration of the crystal in the solvent, and c the actual concentration.

The radius of the critical nucleus, ρ_c, is defined by the condition that $d\Delta G/dr = 0$, and nuclei smaller than ρ_c will shrink while larger ones will grow. Therefore the condition for the formation of critical nucleus is

$$\frac{2\pi \rho_c . h}{\Omega} . \Delta\mu_o + 2\pi h . \gamma = 0 \qquad \text{(iii)}$$

$$\rho_c = -\frac{\Omega\gamma}{\Delta\mu_o} = -\frac{\Omega\gamma}{kT \ln c/c_o} \qquad \text{(iv)}$$

The activation energy for two-dimensional nucleation on a perfect surface is

$$\Delta G = -\frac{\pi\gamma^2 \Omega h}{kT \ln c/c_o} \qquad \text{(v)}$$

<u>Two-dimensional nucleation at a dislocation</u>:

Since a dislocation has strain energy associated with it, the free energy for formation of a two-dimensional nucleus will be less than that for a perfect surface.

$$\Delta G = \frac{\pi r^2 h}{\Omega} \Delta\mu_o + 2\pi r h . \gamma - hE(r) \qquad \text{(vi)}$$

where $E(r)$ is the strain energy within a cylinder of radius r, per unit

length of the dislocation line. The strain energy is equal to the sum of the elastic strain energy and the core energy E_c.

The elastic strain energy for a dislocation is given by (16)

$$E = \frac{G'b^2}{4\pi(1-\nu)} \ln \frac{r}{r_o} \quad \text{(for edge)} \qquad \text{(vii)}$$

$$E = \frac{G'b^2}{4\pi} \ln \frac{r}{r_o} \quad \text{(for screw)} \qquad \text{(viii)}$$

where G' is the elastic shear modulus of the crystal, b the Burgers vector, r_o the radius of the core, ν the Poisson ratio, and r the outer limit of integration in calculating the energy. (If there is a single dislocation in a crystal, r is the radius of the crystal; otherwise it is taken to be equal to the average spacing between dislocations.)

The strain energy of the dislocation can therefore be written as

$$E(r) \lesssim E_c + \frac{G'b^2}{4\pi} \ln \frac{r}{r_o} \qquad \text{(ix)}$$

Since $E(r) > 0$, it is obvious that the activation energy for two-dimensional nucleation at a dislocation site will be lower than that on a perfect surface. Cabrera, Levine and Plaskett (13,17,18) have treated this problem by taking into account only the elastic strain energy.

$$\Delta G = \frac{\pi r^2 h}{\Omega} \Delta\mu_o + 2\pi r h.\gamma - \frac{G'b^2 h}{4\pi} \ln \frac{r}{r_o} \qquad \text{(x)}$$

The condition for the formation of the two-dimensional nucleus is $d\Delta G/dr = 0$. Differentiating equation (x) with respect to r and equating it to zero

$$\frac{2\pi h.\Delta\mu_o}{\Omega} . r^2 + 2\pi r h.\gamma - \frac{G'b^2 h}{4\pi} = 0 \qquad \text{(xi)}$$

This quadratic equation in r gives two solutions

$$r_1 = \frac{\rho_c}{2}\left[1 - \left(1 - \frac{4r_c}{\rho_c}\right)^{1/2}\right] \qquad \text{(xii)}$$

and

$$r_2 = \frac{\rho_c}{2}\left[1 + \left(1 - \frac{4r_c}{\rho_c}\right)^{1/2}\right] \qquad \text{(xiii)}$$

where $r_c = G'b^2/8\pi^2\gamma$. There is a maximum at r_2 and a minimum at r_1. The results are meaningful only outside the core region, i.e. when r_1, r_2 and ρ_c are greater than r_o; r_1 and r_2 are finite only when $4r_c/\rho_c < 1$.

Cabrera and Levine (13) point out that as $\Delta\mu_o$ is increased by decreasing c/c_o, r_1 and r_2 approach each other and finally when $\rho_c = 4r_c$, r_1 becomes equal to r_2. They interpret this as meaning that at sufficiently great undersaturations (low c/c_o) the dislocation core 'opens up' spontaneously and there is no need to nucleate new layers.

One disadvantage of the above treatment is that it does not take into account the core energy of the dislocation - an error which will be serious when dislocations with Burgers vector of a unit spacing are considered (13). The error is especially important for crystals with a low surface energy and hence a small value for ρ_c. Although it appears that etchpits at edge dislocations and perhaps also at screw dislocations are formed by rapid two-dimensional nucleation, there is yet no suitable detailed theory for this process.

Dissolution at a screw dislocation:

A dissolution spiral will tend to form as atoms are removed from the step at a screw dislocation. Burton et al. (7) developed the theory

of a spiral on a growing crystal and they have shown that the distance, y_o, between successive turns of the spiral is given by

$$y_o = 4\pi \rho_c \qquad \text{(xiv)}$$

Cabrera and Levine (13) repeated the calculation for an evaporating crystal, taking into consideration the elastic strain energy of the dislocation, and proved that

$$y_o = 19 \rho_c \qquad \text{(xv)}$$

Substituting the value for ρ_c

$$y_o = - \frac{19\gamma\Omega}{kT \ln c/c_o} \qquad \text{(xvi)}$$

This clearly shows that the spacing of the ledges depends on undersaturation.

By assigning suitable values to the parameters in equation (xvi), a nominal value for the spacing between ledges can be calculated, and from this value the minimum value for the slope of the pit can be computed. Johnston (19) has shown that the slope of the pits in the case of lithium fluoride is about 2^o. Pits of this slope should be visible with interferometric techniques. Ives and Hirth (20) have found that the slopes of the pits formed at screw dislocations in the case of LiF vary from 5^o to 12^o.

The inhibited dissolution of lithium fluoride:

The principal controlling factors in the etching of lithium fluoride by a dilute aqueous solution of ferric fluoride are the diffusion field of dissolved lithium fluoride and the inhibition offered by ferric ions. The inhibitor will control the surface-reaction stage, the act of severing the chemical bonding of the ions of the crystal; diffusion field will control

the liquid-diffusion and surface-diffusion stages, the process of transport of dissolved ions away from the crystal surface.

The diffusion problem for the dissolution of crystals has been analysed by Burton et al. (7). They have calculated the rate of advance of monomolecular steps by equating the sum of the steady state hemispherical diffusion fluxes around the kinks in a ledge to the steady state semicylindrical diffusion flux around the ledge and the sum of the semicylindrical fluxes from the ledges to the planar diffusion flux into the solution through the unstirred layer of the liquid adjacent to the surface. At high undersaturation their treatment yields the steady state velocity of a parallel train of ledges

$$v_{\infty} = \frac{D(c_o - c)\Omega y_o}{h\delta} \qquad \text{(xvii)}$$

where D is the diffusion coefficient of lithium fluoride, h the height of the monomolecular ledge, and δ the thickness of the unstirred layer of the solution adjacent to the crystal. The above treatment assumes that the thickness of the unstirred layer, δ, is much greater than the steady state ledge spacing y_o. There is some reason to suppose that the unstirred layer is only a few A° thick (21). Under this condition it is likely that the motion of the ions on the surface, rather than directly into the solution, will be the limiting step to the diffusion of matter from the ledges. Hirth and Pound (15) have solved this problem and their treatment yields the ledge velocity

$$v = \frac{\left[(2\bar{X}/h)\ \tanh\ (y_o/2\bar{X})\right] D\Omega(c_o - c)}{\delta} \qquad \text{(xviii)}$$

where $\bar{X}$ is the mean diffusion distance.

The ledge velocity, v, approaches its terminal value, v_∞, asymptotically as the hyperbolic tangent approaches unity as its argument increases beyond $\backsim 3$. The crystal ledges, therefore, accelerate at small values of y_o until the maximum v_∞ is attained when $y_o/2\bar{X} \backsimeq 3$.

The limiting value is given by (20)

$$v_\infty \backsimeq \frac{D\Omega(c_o - c)y_o}{38h} \qquad \text{(xix)}$$

The slope of the pit at the source is

$$\frac{h}{y_o} = \frac{hkT \ln c_o/c}{4\pi\gamma\Omega} \qquad \text{(xx)}$$

If y_o exceeds $6\bar{X}$, the ledges will maintain a constant spacing, and the slope of the pit will remain constant. If y_o is less than $6\bar{X}$, the ledges will accelerate and the pit will become less steep as the distance from the source increases approaching a limiting value of $h/6\bar{X}$.

The spacing at an edge dislocation source depends on the hole-nucleation probability at the dislocation, since no perpetuating ledges are associated with an edge dislocation. However, as long as a high undersaturation is maintained, there is no barrier to nucleation at edge dislocations and the kinetics of ledges emanating from such a source will be analogous to the kinetics treated above.

The presence of a poison at a crystal surface affects surface free energy, γ, and the effective saturation concentration c_o. The deposition of an inhibitor at a crystal ledge will lower surface free energy, altering it to a new value, γ'. Since the equilibrium crystal slope is inversely proportional to the surface free energy, the presence of an inhibitor can

produce an increase in slope. By adsorption at the kink sites, the poison can hinder the dissociation of molecules from a ledge so that the concentration of the solute maintained at a kink is reduced. This will reduce the undersaturation of the solvent for a given concentration of solute and c_o will have to be replaced by c_o' where $c_o' < c_o$. Under these conditions the equation for pit slope, i.e. equation (xx), will assume the form

$$\frac{h}{y_o} = \frac{hkT \ln c_o'/c}{4\pi\gamma' \Omega} \qquad \text{(xx(a))}$$

Ives and Hirth(20) have found that in the inhibited dissolution of lithium fluoride in the presence of ferric ions equation (xx(a)) is not obeyed. They could only reconcile the results with the theory by assuming a time-dependent ledge poisoning.

Topographical theory:

Frank (8) considered the process of dissolution of a crystal as a progression of unit steps, each of height h across a reference face of a crystal. He assumed that the speed with which a step moves depends, among other things, on the proximity of other steps, i.e. upon the localised step density (whereas, strictly, a density of discrete entities cannot be defined at a point). This dependence of ledge velocity on ledge density was adapted from the work of Lighthill and Whitham (22) who applied this principle to the flow of highway traffic and river floods.

Let k be the step density, i.e. the number of steps per unit length in the neighbourhood of a particular point, and q be the step flux, the number of steps passing that point in unit time. Then

$$\text{surface slope} = hk = \frac{\partial y}{\partial x} \qquad \text{(xxi)}$$

Dissolution rate normal to the surface $= -\frac{\partial y}{\partial t} = hq$ (xxii)

The basic postulate $q = q(k)$ defines two velocities

$v(k)$, the mean speed of an individual step $= \frac{q}{k}$ (xxiii)

and

$c(k)$, the kinematic wave velocity $= \frac{dq}{dk}$ (xxiv)

The continuity equation for the conservation of steps is given by

$$\frac{\partial q}{\partial x} + \frac{\partial k}{\partial t} = 0 \qquad \text{(xxv)}$$

i.e.
$$\frac{\partial q}{\partial k} \cdot \frac{\partial k}{\partial x} + \frac{\partial k}{\partial t} = 0 \qquad \text{(xxvi)}$$

$$c(k) \cdot \frac{\partial k}{\partial x} + \frac{\partial k}{\partial t} = 0 \qquad \text{(xxvii)}$$

In the (x,t) plane along a line of slope $c(k) = dq/dk = dx/dt$, k is constant and therefore q is constant; this line is called a characteristic.

Geometrically the sequence of crystal profiles $y = y(x)$ at a sequence of times t, defines a surface $y = y(x,t)$. The characteristics correspond to the lines on this surface which by equation (xxvii) have straight line projections on the (x,t) plane. These characteristics also project as straight lines on the (x,y) plane, since

$$\frac{dy}{dx} = \frac{\partial y}{\partial x} + \frac{\partial y}{\partial t} \cdot \frac{\partial t}{\partial x} = h\left(k - \frac{q}{c}\right) \qquad \text{(xxviii)}$$

which is a constant.

These concepts are summarised in a simple geometrical construction from a probable relationship of $q = q(k)$, Figure 2, showing the direction of the trajectory of a point of given orientation in accordance with equation (xxviii).

A discontinuity in slope for adjacent densities k_1 and k_2 (for which the corresponding fluxes are q_1 and q_2) follows a trajectory in the (x,t) plane of slope

$$\frac{dx}{dt} = \frac{q_2 - q_1}{k_2 - k_1} \qquad \text{(xxix)}$$

and in the (x,y) plane of slope

$$\frac{dy}{dx} = h\left[k_1 - q_1\left(\frac{k_2 - k_1}{q_2 - q_1}\right)\right]$$

$$= h\left[k_2 - q_2\left(\frac{k_2 - k_1}{q_2 - q_1}\right)\right] \qquad \text{(xxx)}$$

The edge trajectories are not necessarily straight.

From the above calculations where the dissolution velocity is defined as measured normal to the macroscopic surface of the crystal rather than normal to the microscopic crystallographic terraces, Frank introduced the basic theorems of his topographical theory of dissolution.

Theorem 1: If the rate of dissolution of a crystal surface is a function only of orientation (or depends on time only through an orientation independent factor) then the locus in space of a particular orientation of a crystal surface on dissolution is a straight line. The orientation dependence of the etch rate allows the complete dissolution properties of the crystal in a given solvent to be described in terms of a polar diagram of the reciprocal normal etch rate as a function of orientation, yielding a polar reluctance diagram.

Theorem 2: The vector defining the locus in space of a given crystal surface orientation is parallel to the normal drawn from the reluctance

surface at the corresponding orientation.

These theorems have been derived by adopting a two-dimensional approach but they also hold good for three-dimensional cases. The theorems have been shown to apply to the dissolution of germanium by Frank and Ives (23) and of lithium fluoride by Ives (24). Ives and Hirth (20) have found that dissolution at dislocation etch pits in lithium fluoride dissolving in aqueous solutions containing ferric ions does not follow the kinetic laws predicted by Frank's topographic theory or the mechanistic approach of Burton, Cabrera and Frank (7). Their results were explained on the basis of the mechanistic approach, invoking the concept of a time-dependent adsorption of the poison at the ledges.

Frank (8) investigated the profiles of step bunches, using his dissolution theorems. Figure 3 shows a surface having a low density of steps except in one region where there is a bunch of high density initially symmetrical. Assuming that q depends on k qualitatively, as shown in Figure 2, the characteristics for low values of k have smaller slope than those for higher values of k. The characteristics diverge at the leading edge, while at the trailing edge they converge and ultimately meet. Where they meet, the intervening density values vanish and an edge develops. At a later time t, the bunch of steps has assumed the density distribution shown as $k(x,t_1)$ in the figure. The bunch has travelled to the right with a velocity given by $c(k)$. The crystal profiles are shown in the figure.

Whatever the initial profile in the bunch, it will ultimately develop a discontinuity of slope at the rear as long as d^2q/dk^2 is negative. When d^2q/dk^2 is positive, the discontinuity in slope is developed at the leading edge of the bunch (as shown in Figure 4). When q depends on k in the

simplest way, by interference through the diffusion fields of neighbouring steps, this cannot occur except for very steep slopes, approaching other low-index crystallographic surfaces (8). It is this condition of a positive value for d^2q/dk^2 that is important in etching to produce well defined etch pits.

The reversal in the curvature of the q vs. k plot can be accomplished by the effect of impurities. The impurities must be present in very small concentrations in order to exhibit a time-dependent surface adsorption requiring a very long time for adsorption equilibrium to be established. It must be rendered ineffective upon passage of a dissolution step. The adsorbed impurity inhibits the motion of steps and the reduction in velocity of the steps is a function of the preceding terrace width. The density of adsorption met by an oncoming step is a function of the time elapsed, $1/q$, since the passage of the previous step. If dq/dk is positive, steps are more impeded by the impurity effect when they are farther apart than when they are close together. This effect can make a positive contribution to d^2q/dk^2. Since for small values of k, d^2q/dk^2 has only a small negative value, even a mild impurity effect can transfer the discontinuity from the rear to the front of the bunch. Frank (8) generalised this effect by indicating "All etchants which produce well-marked etch pits contain traces of protective substance either by chance or by design".

Summing up, it can be said that when d^2q/dk^2 is positive, then macroscopic ledge formation is stabilised; for negative values of d^2q/dk^2 no pile up is stable and smooth dissolution features will be observed. These postulates have been verified by Hulett and Young (25) in the electrolytic dissolution of copper in electrolytes containing hydrochloric and hydrobromic

acids. Smooth surfaces corresponding to a negative value for d^2q/dk^2 are observed at high current densities and low Br^- concentrations, and macroscopic ledges are stabilised (corresponding to a positive value for d^2q/dk^2) at low current and high Br^- concentrations.

Frank (8) has also shown that an important effect brought about by the presence of impurities is the 'bunching' of steps. This can be followed with the help of Figure 5. A regular sequence of steps is disturbed by allowing one step (c) to lag behind its regular position. Since it meets a dirtier surface, it is retarded. The step (b) accelerates a little because it has less interaction through the diffusion field of (c). The step (d) suffers diminished impurity retardation and catches up with (c). The united pair (cd) lag increasingly behind (b). The terrace (bc) lengthens continuously and a bunch of steps (cde) forms behind it. The regular sequence of steps thus exhibits a strong tendency for bunching. Once a macroscopic step is formed by bunching, it will continue to increase in height as long as single steps are fed into it, while few, if any, monatomic steps will move through the bunch (26). The velocity of the macroscopic step will be determined by the velocity of the leading step.

The continuum kinematic theory of Frank (8) characterises all steps in a small bundle by the same density k and flux q; it cannot adequately describe any changes in step distribution that depend on large or quantitative differences in the behaviour of adjacent step intervals. Mullins and Hirth (27) have shown that while the leading edge diverges uniformly in accordance with the kinematic theory, the trailing edge breaks up pairwise into a set of double ledges in a disturbance that propagates through the entire train, rather than continuously converging, as the kinematic theory would predict.

CHAPTER II

DISLOCATION ETCH PITS IN LITHIUM FLUORIDE

When a crystal dissolves in a solvent, material is preferentially removed from the kink sites where binding is the weakest. The concentration of kinks in a ledge depends on temperature and effective undersaturation in the solvent. The necessary conditions for dissolution to occur are, therefore, a constant source of ledges on the surface of a crystal and a solvent in which the crystal is appreciably soluble. In the absence of any constraints, the kinks travel fast until they are annihilated, thereby resulting in the formation of smooth dissolution features. In order to produce well defined etch pits on the surface, it is necessary to slow down the rate of nucleation and motion of kinks and this can be done by the introduction of an inhibitor in the solvent. Since a dislocation provides a constant source of steps, etch pits can be formed more easily at the sites of intersection of dislocations than in any other region on the surface.

The etchants which have been developed for the formation of dislocation etch pits on the cleavage faces of lithium fluoride are based on water or hydrofluoric acid as solvent with a small amount of the inhibitor.

The aqueous etchant for lithium fluoride:

Gilman, Johnston and Sears (28) have carried out extensive investigation on the formation of etch pits in lithium fluoride and they have concluded that for an etchant to produce uniform crystallographic etch features, there must be present a few parts per million (p.p.m.) of inhibitor

ion. Furthermore, of some thirty cations investigated, only Fe^{+++} and Al^{+++} were found effective in this respect. These workers have suggested that three conditions must be fulfilled for successful inhibition. The cation must be of similar ionic radius to that of the cation of the lattice; there must be a stable fluoride complex of the cation; the metal fluoride should be relatively insoluble in water. Gilman et al. (28) have also shown that the valence of the cation is not important regarding its effectiveness as an inhibitor and that anions which form ferric complexes more stable than the fluoride complex disrupt the etching action.

The accepted etchant for lithium fluoride is an aqueous solution containing 3 to 4 p.p.m. Fe^{+++} as ferric chloride or ferric fluoride (acidified to a $p_H \backsim 3$ to prevent precipitation of ferric hydroxide). This etchant has been referred to as the 'W' etchant (29,30) and is used to study the mechanical properties of lithium fluoride by revealing the sites of intersection of dislocations with the crystal surface through the formation of etch pits. The etch pits formed have their edges parallel to $\langle 100 \rangle$ directions and the surfaces forming the pit are of the $\{okl\}$ type (Figure 6a) (29,30).

The shapes of etch pits reveal the type of dislocation at which they have developed. The glide plane in lithium fluoride is $\{110\}$ and the glide direction is $\langle \bar{1}10 \rangle$. Edge dislocations will emerge at glide bands which lie in a $\langle 110 \rangle$ direction and screw dislocations will emerge at glide bands which are parallel to a $\langle 100 \rangle$ direction. Therefore, on the $\{100\}$ cleavage planes, edge dislocations will give rise to symmetrical etch pits while screw dislocations will form asymmetric pits. The 'W' etchant distinguishes between fresh and aged dislocations by forming more distinct pits at the former (28).

Acid Etchants:

The first etchant to be developed for the formation of dislocation etch pits on the surfaces of lithium fluoride was a modified CP-4 solution containing equal parts (by volume) of concentrated hydrofluoric acid and glacial acetic acid saturated with ferric ions (30). This etchant has been referred to as the 'A' etchant. It produces etch pits with their edges parallel to $\langle 110 \rangle$ directions and the surfaces of the pits are of the $\{hhl\}$ type (29) (Figure 6b). Unlike the neutral etchant, the 'A' etchant cannot distinguish between fresh and aged dislocations (30).

A simplified acid etchant, consisting of an aged solution of ferric fluoride in reagent grade hydrofluoric acid, has been developed by Ives (29). This etchant produces pits of the $\{hhl\}$ type, but has an inconveniently fast action.

Polar molecule inhibitors:

Westwood et al. (31) have employed aqueous solutions of long chain fatty acids and perfluoroacids to develop etch pits on the cleaved surfaces of lithium fluoride. The adsorption of the polar molecule at the kink sites results from the attraction of the dipole end of the polar molecule - the carboxyl group towards unneutralised charges at the kink. The stability of the complex formed by adsorption depends on the chain length of the molecule, the nature of the solvent, the concentration and degree of saturation of the polar molecules present in the solvent, the solubility of complex in the solvent, the temperature and degree of agitation in the system. Empirically, as the chain length increases and the concentration of polar molecules in solution increases, so does the stability of the complex in the solvent.

As the solubility of the complex in the solvent, the temperature and the degree of agitation increase, the stability of the complex decreases (31).

A point of interest is that etch pits produced on dislocations in myristic and stearic acid solutions are flat-bottomed initially. After a certain etching time, depending on the concentration and chain length of the adsorbing molecule, the pits become pyramidal. This behaviour is supposed to result from chemisorption and complex formation with the ions surrounding the core of the dislocation itself which will affect the core energy available for the nucleation of kinks (31).

Kink kinetics and etch pit morphology:

Dissolution proceeds by the removal of ions from kink sites. It is therefore natural to expect that the kinetics of dissolution and the shape of etch features will be governed by the rate of nucleation of kinks and their subsequent motion.

The rate of nucleation of kinks depends on temperature and effective undersaturation of the solution. For a given temperature, it is obvious that the greater the solubility of the crystal in the solvent the higher will be the kink nucleation rate; for example, since the solubility of lithium fluoride is greater in hydrofluoric acid than in water, the rate of kink nucleation will be higher in the system lithium fluoride - hydrofluoric acid than in lithium fluoride - water. The adsorption of an inhibitor at a kink site hinders the removal of material and thereby increases the mean life-time of a kink. Taking into consideration the two parameters, the time for nucleation of a kink pair and the mean life-time of a kink, it is possible to explain the formation of different etch morphologies.

Ives (29) has suggested two basic categories of kink kinetics in the dissolution of lithium fluoride:

Type 1 - Little inhibition. If the mean time for kinks to sweep a length of ledge is less than the time between successive kink nucleation in that length, unkinked ledges are stable. Their motion is then only dependent on the kink nucleation rate. Ledge surface results, which corresponds to {okl} faced etch pit of the 'W' etchant.

Type 2 - Greater inhibition. When kinks are nucleated at a rate greater than they can clear the ledges, they will tend to pile up. Kink surfaces are produced and in the limit maximum kink density will result in {hhl} surfaces as observed with the 'A' etchant.

By combining the etchants and varying their composition, Ives (29) was able to determine the roles of the various components. Hydrofluoric acid was seen to increase the nucleation rate of kinks increasing the effective undersaturation, and the addition of acetic acid was found to reduce the solubility of lithium fluoride thereby introducing an opposing effect.

Ives (29) has found that the nucleation rate has been affected by the inhibitor, especially at reduced undersaturations - an effect that has been confirmed by Sears (32) for the growth of lithium fluoride in solutions containing ferric ions as inhibitors.

Etch morphologies in lithium fluoride with 'W' etchant:

The etch features obtained in the dissolution of lithium fluoride in water with varying concentrations of iron is shown in Figure 7. At very low concentrations of iron, the attack is rough and

irregular etch features are observed (Figure 7a). As the concentration of the inhibitor is increased, the features become more and more regular and corresponding to an optimum concentration of iron (2 to 3 p.p.m.) well defined etch pits of the {okl} type are observed (Figure 7c). When the concentration of iron is increased further, there is at first a tendency for the pits to become rounded at the edges (Figure 7d) and ultimately the pits are conical (Figure 7e).

In order to understand the action of ferric ions in this system, radiotracer experiments using Fe^{59} have been carried out by Ives and Baskin (33) and adsorption isotherms for iron chemisorbed onto the surfaces during etching have been established. Their results indicate that the mean coverage of iron for the formation of regular {okl} pits is equivalent to a fraction (1/25) of a monolayer. There is also a point of inflexion at a bulk iron concentration corresponding to the optimum condition for good, plane-sided pyramidal pits. The point of inflexion in the isotherm has been related to the filling up of the kink sites by iron, a condition referred to as 'monokink' coverage (33).

At inhibitor coverage less than monokink, kinks will be unequally inhibited. Hence some kinks will quickly traverse their ledges while others will be held up by the inhibitor. This will give rise to irregular dissolution features. When monokink coverage is obtained, all kinks are equally constrained and crystallographically well defined pits are formed. The barrelling of the etch features and their approach to conical shape at higher concentrations of iron have been explained by introducing the concept of diffusion control (33).

Ives and Baskin (33) postulate that once monokink coverage is

obtained, the rate of formation of complexes of ferric ions in solution (in the stagnant boundary layer or loosely associated with the surface) becomes comparable to that of attachment of ferric ions at other surface sites. This increase in the concentration of the complex in solution increases the barrier to diffusion of soluteaway from the surface. When dissolution is subject to diffusion control, the dissolution sites interact through the diffusion fields centred on them and they repel each other. This gives rise to kink pile ups and eventually to the attainment of conical features - a condition corresponding to complete diffusion control, since all crystallographic features have been eliminated.

The concepts of inhibitor and diffusion control in the dissolution of lithium fluoride are mainly based on interference microscopic studies of dissolved surfaces and adsorption isotherms for iron chemisorbed onto the surface. In order to have a better understanding of these rate controlling mechanisms, it is necessary to study the shapes of monatomic ledges in etch pits. The only way of reaching such a high resolution is by resorting to electron microscopy. Electron microscopic study of the etch pits can be carried out by the replication technique. The gold decoration technique developed by Bassett (34) for revealing monatomic ledges on the cleaved surfaces of ionic crystals can also be tried.

CHAPTER III

EXPERIMENTAL PROCEDURE

The fine structure of etch pits formed on the cleavage faces of lithium fluoride can be resolved by electron microscopy. Specimens for electron microscopic examination can be prepared in two ways: (a) by replicating the surface, and (b) by thin film techniques. Thin foils permit a direct insight into the interior of metals and alloys; they show up the nature and distribution of defects and they are suitable for electron diffraction. On the other hand, replicas help in the study of surfaces alone and their resolution is not as high as that with thin films. It is not possible to examine thin films of lithium fluoride in the electron microscope since they volatilise spontaneously when bombarded by the electrons. Therefore the only way of studying the fine structure in etch pits is to use the replication technique.

Methods of replication:

A replica may be defined as a thin film which presents to the electron beam locally varying thicknesses and topography which correspond in some manner to the surface detail. The manner in which the thickness differences correspond, and hence the interpretation of density variations in the micrographs, depends on the method of replication. Surface replicas for electron microscopy were first suggested by Mahl.[47] Replicas can mainly be divided into three groups:

(a) electrolytic or thermal oxide replicas,

(b) plastic replicas, and

(c) evaporated films and oxides.

Evaporated film replicas, particularly pre- or post-shadowed carbon replicas are the most frequently used ones. Table I summarises the characteristics of the various replicas.

Oxide film replicas can be used for studying the surface structure of a number of metals like copper, aluminum, iron, nickel, etc. In iron and some special steels the surface can be oxidised by heating in air or other atmospheres (35); aluminum can be oxidised by the anodising technique employing an electrolytic bath of acidified disodium hydrogen phosphate. Wherever there is difficulty in oxidising the surface, aluminum can be used as a moulding material for getting the impression, the oxide film being then formed and detached as a type of two stage replica (36). The oxide film replicas are crystalline in nature and much of the detail observed is due to diffraction effects.

Plastic replicas are formed by applying a small quantity of a solution of formvar* or collodion in amyl acetate and mechanically stripping the film after it has dried. The success in stripping thin plastic films from a surface is dependent both on surface roughness and on the presence of thin foreign layers that reduce adhesion. Plastic replicas are complicated by lack of dimensional stability of the polymer, relatively poor contrast and thickness variations of the film. These defects are removed to a great extent by shadow casting in which metal is evaporated at an

---

* Formvar is polyvinyl formal. A solution of formvar in amyl acetate or ethylenedichloride can be used in the preparation of plastic replicas.

TABLE I

CHARACTERISTICS OF THE REPLICAS

Type of Replica	Intrinsic Resolution	Interpretation	Permits Repetition	Stability under electron irradiation	Technique of Preparation
Electrolytic or thermal oxide	Good; ~100 Å	Good	No; surface destroyed	Good	Simple; but not generally applicable
Plastic	Poor; >200 Å	Excellent; but limited	Yes	Poor	Simple; but not applicable to particles
Evaporated films (elements and oxides)	Good to best; 10 - 200 Å	Yields greatest information	Yes; except for high resolution	Good to best	More complex; but of general applicability

(Adapted from R. D. Heidenreich and C. J. Calbick, "Physical Methods in Chemical Analysis", Vol. 1. Academic Press, New York and London, 1960, p. 582.)

angle onto the surface of a thin plastic replica. Since the plastic replica is a mould of the sample surface, the evaporated metal film forms a positive replica of the surface. The scattering power of the plastic film for electrons is small compared to that of the metal. Therefore the resulting electron micrographs are typical of evaporated film replicas except in regions in which, as a result of surface topography, no metal is deposited (i.e. within shadows).

Evaporated film replicas:

Evaporated film replicas are obtained by evaporating a suitable element or oxide onto the surface of interest and then stripping the film. The polystyrene-silica replica was the first application of vacuum evaporation to the production of replicas for electron microscopy (37). The evaporated film replicas can be produced in one step by evaporating straight onto the surface or in two steps by first forming a plastic film on the surface and then evaporating the material onto the stripped plastic film. Usually carbon or silicon monoxide is used for evaporation in preparing single stage replicas. Lack of crystallinity is an outstanding virtue of carbon and silicon monoxide replicas. Silicon monoxide is generally used where a high strength thin film is required or where the surface to be replicated is very rough. Very often the evaporated films formed may be composed of two different materials. The first component, in these cases, forms the base film and is usually deposited at normal incidence; the other, the shadowing material, is deposited at an angle to the surface normal. Shadowing improves the contrast of the replica and at the same time provides a three dimensional effect.

Evaporated films are generally stable in the electron beam because they have good electrical conductivity. Plastic films often curl up when under observation. Electrostatic charging (which occurs with non-conducting films) and local heating contribute to this effect. Within the range of thickness useful in replicas, heating is proportional to film thickness and the thinner films are more stable under electron microscope observation than thicker films. Stability is also affected by high residual gas pressure during evaporation. Superiority in this respect is the most important advantage of carbon films. Certain other materials, like silicon, germanium, zirconium and aluminum, also exhibit good stability and conductivity. Metal-shadowing of non-conducting films such as SiO, SiO_2, TiO_2, Al_2O_3 and plastic improves stability. Unshadowed inorganic films are more stable than plastic.

Contrast in electron micrographs is produced by variations in thickness of the replica. The relation of thickness variations in the replica to the corresponding surface features depends on the material employed for replication and in particular whether the replicating material migrates over the surface during condensation. When every atom sticks where it strikes, as with metals, the replica is uniformly thick in the direction of the source; and if this direction is the same as that of the incident electron beam, the only intensity variations observable are those due to the crystalline structure. Hence, to provide contrast due to surface topography, the metal beam must be incident at an angle with the surface normal. The migratory components of the oxides and Group IV elements, on the other hand, tend to form a film of uniform thickness normal to the local surface; and hence the thickness in the electron beam varies with the local slope. If the metal is evaporated at an angle, thickness variations required for replication occur through the formation of shadows.

Crystallinity of metal films introduces granularity into micrographs which is not related to the surface structure. Crystallite size varies greatly for different metals. Gold and silver yield large crystals when the thickness of films exceeds 200 Å. In general the higher the melting point of the shadowing material, the smaller are the crystals formed. Metals which evaporate at a low temperature produce more background structure than those with opposite characteristics. Platinum is the best material in this respect. It has also a high scattering cross-section for electrons and thereby gives rise to good contrast. Because of difficulty in evaporating platinum from a tungsten filament (platinum alloys with tungsten), platinum-palladium alloys are sometimes used. Where a high resolution is necessary, preshadowing with platinum to an average thickness of 10 Å to 20 Å followed by evaporation of carbon to a thickness of about 50 Å is preferable (38).

For very high resolution work where no discrete crystallites are permissible, the simultaneous evaporation of platinum and carbon, the method developed by Bradley (39), constitutes the best method. An amorphous deposit is obtained in this case; the resolution is limited by any background structure that is present. The background structure is probably caused by the contaminating layer of hydrocarbons found in demountable vacuum systems, limiting the resolution to about 20 Å (39). Monomolecular steps in cleaved crystals of sucrose have been revealed by this method (39).

The brief survey of the replication techniques suggests that evaporated replicas, particularly the platinum-carbon replicas, will be best suited for the fine structure resolution of etch pits on the cleavage surfaces of lithium fluoride. Another method which is of considerable

importance is the gold decoration technique developed by Bassett (34) and referred to as the Decoration Replica technique by Kay (40).

Decoration replicas:

The structure and properties of thin films and the phenomena of Epitaxy and nucleation and growth have been studied to a very large extent by evaporating metals onto the surfaces of suitable substrates. The substrates generally employed are cleaved surfaces of ionic crystals and mica.

When gold is evaporated into the surface of cleaved sodium chloride crystal , it has been found that at very small thickness of gold there is preferential nucleation at steps on the substrate surface (34). This gives rise to a very pronounced decoration effect which is invaluable for revealing the step structure on rock salt. The steps act as preferential sites for nucleation of gold even when they are only monatomic in height, as Bassett (34) was able to show by measuring the total height of a staircase of steps, by means of the displacement of a surface slip step crossing the staircase. There is no evidence that the orientation of the nuclei on the steps is any different from the nuclei which form on the apparently smooth parts of the surface. Bassett, Menter and Pashley (41) have shown that when the thickness of gold is gradually increased the crystallites initially grow in size with the simultaneous tendency for the preferential growth on steps to disappear.

It has been found that elevated substrate temperatures are necessary for orientation to occur. Bruck (42) deduced that many metals orient on rock salt only above a certain temperature which is characteristic of the particular metal. The validity of this conclusion is open to doubt as a result of the work of Kehoe (43) who found that orientation of gold on

sodium chloride occurs in the temperature range 130°-300°C, although Bruck determined the characteristic temperature as 400°C. Bassett (41) has obtained a good orientation of gold on rock salt at a substrate temperature of 270°C. The general conclusion that can be drawn from these observations is that elevated temperatures are necessary for orientation to occur but the appropriate temperature depends on the nature of the metal deposit and the substrate.

The fact that the nucleation of gold occurs preferentially along the steps, when small quantities of gold are evaporated, forms the basis for the decoration replicas.

Kay (40) has suggested the following procedure for revealing the monatomic steps on cleaved surfaces of ionic crystals:

(1) A freshly cleaved surface of the crystal under examination is coated with 5-10 Å of evaporated gold in a vacuum unit containing two sources of heat, one for gold and the other for carbon. It is necessary to heat the crystals since aggregation of gold particles does not always occur at room temperature.

(2) A carbon film of thickness 50-100 Å is deposited on gold, preferably without breaking the vacuum.

(3) The carbon film with the gold particles attached is floated onto water or onto the surface of a suitable solvent which dissolves the crystal.

(4) Pieces of the film are picked up on support grids and examined in the electron microscope.

Bethge (44) has extensively applied the decoration technique to the thermal etching of alkali halides; the technique has also been utilised by Hennig (45,46) in the study of vacancies and dislocations on the cleaved surfaces of graphite, by etching the cleaved surfaces of graphite with O_2,

Cl_2 or CO_2 and decorating the etched surface with minute quantities of gold.

Contrast in replicas:

The development of an understanding of contrast in electron images is based on the scattering of electrons by the object. A point in the object scatters incident electrons over a range of angles with the scattered intensity generally falling off with increasing angle. The distribution in intensity with scattering angle is described by the differential cross-section, which can be defined in terms of the number of electrons, dn, scattered per unit time from incident intensity I_o per unit solid angle Ω.

$$\frac{dn}{I_o} = D(\Omega)\, d\Omega \qquad \text{(xxxi)}$$

The differential cross-section $D(\Omega)$ is related to the total cross-section per atom σ by the expression

$$D(\Omega) = \frac{d\sigma}{d\Omega} \qquad \text{(xxxii)}$$

σ represents the total fraction of the incident electrons scattered outside a certain minimum angle. The solid angle Ω and scattering angle β are related by

$$\Omega = 2\pi (1 - \cos \beta) \qquad \text{(xxxiii)}$$

Therefore

$$d\Omega = 2\pi \sin \beta d\beta \qquad \text{(xxxiv)}$$

The total cross-section per atom for scattering outside β_{min} is

$$\sigma_{atom} = 2\pi \int_{\beta_{min}}^{\pi} D(\beta) \sin \beta d\beta \qquad \text{(xxxv)}$$

The value for β_{min} is the half angle of the objective, β_{obj}.

To calculate the intensities in electron images, the above integral must be evaluated to obtain the single atom cross-section, and a summation of the latter gives the cross-section for the solid.

If the presence of neighbouring atoms in a solid does not affect the scattering cross-section of an atom, the total cross-section, Q, for an object containing N atoms/cm^3 is given by

$$Q = N\sigma_{atom} \qquad \text{(xxxvi)}$$

$$= \frac{N_o}{M}\sigma_{atom}\rho \qquad \text{(xxxvii)}$$

where N_o is the Avagadro number, ρ the density, and M the molecular weight of the substance.

When the thickness of the object is t, Qt determines the scattering of electrons by the object. It is the mass thickness of the object. The mass thickness interpretation for intensity variation holds for replicas which are essentially amorphous in nature. For plastic and carbon replicas, even when shadowed with nearly amorphous metal layers, this interpretation is adequate (47).

Let L be the distance from the specimen to a flat observing screen. Considering an annular area of width dR at radius R, the intensity at R per scattering atom will be

$$I(\beta) = \frac{\text{No. of electrons scattered}}{\text{Area of the ring}} \qquad \text{(xxxviii)}$$

$$\text{Area of the ring} = 2\pi R.dR = 2\pi L^2 \tan\beta d\beta \qquad \text{(xxxix)}$$

$$\text{Therefore} \quad I(\beta) = \frac{I_o D(\Omega)d\Omega}{2\pi L^2 \tan\beta d\beta} \simeq \frac{I_o D(\beta)}{L^2} \quad \text{for small } \beta \qquad \text{(xl)}$$

This simple expression holds good only when there is single scattering. Generally, for large values of mass thickness, plural or multiple scattering occurs; this introduces a change in the distribution of scattered intensity. The critical mass thickness of single scattering can easily be calculated.

Consider a specimen of thickness t. Let the incident surface be $z = 0$. At a depth z in the object, the intensity scattered outside the objective aperture by a thin slab between z and $z + dz$ is

$$dI = -I(z)\, Q.dz \qquad \text{(xli)}$$

The integration of this equation from $z = 0$ to $z = t$ gives

$$I = I_o\, e^{-Qt} \qquad \text{(xlii)}$$

Q represents the number of scattering events per unit distance of travel. Since Q has the dimensions of distance^{-1}, the reciprocal of Q represents the mean free path between collisions, λ.

For an object of thickness t, assuming a Poisson distribution for scattering events, the probability $w(t)$ of b events is

$$w(t) = \frac{1}{b!} \left(\frac{t}{\lambda}\right)^b e^{-t/\lambda} \qquad \text{(xliii)}$$

The condition to be satisfied for single scattering is

$$\frac{d\, w(t)}{d(t/\lambda)} = e^{-t/\lambda} \left[1 - \frac{t}{\lambda}\right] = 0 \qquad \text{(xliv)}$$

Therefore

$$\frac{t}{\lambda} = Qt = 1 \qquad \text{(xlv)}$$

The critical mass thickness is

$$(\rho t)_c = \frac{M}{N_o \sigma_{atom}} = \rho \lambda \qquad \text{(xlvi)}$$

As long as the single scattering approximation holds, the intensity entering the objective aperture from a point in the object is determined by the total cross-section Q and the object thickness t at that point. If the object is of uniform thickness t, the scattering acts at all points are determined by Qt and there is no image contrast. The intensity at the image point is given by

$$I = I_o e^{-Qt} \qquad \text{(xlvii)}$$

If the object has a localised protuberance of thickness Δt, the intensity at an image point from this region of enhanced thickness is

$$I = I_o e^{-Q(t+\Delta t)} \qquad \text{(xlviii)}$$

The intensity change at the protuberance is given by

$$I = I_o e^{-Qt} (1 - e^{-Q \Delta t}) \qquad \text{(xlix)}$$

Contrast is defined as the ratio of $\Delta I/I$ or the intensity change relative to background.

$$\text{Contrast} = \frac{\Delta I}{I} = 1 - e^{-Q \Delta t} \backsimeq Q \Delta t \quad \text{for} \quad Q \Delta t < 1 \qquad (1)$$

The minimum observable contrast in an image is about 5%. The minimum change in thickness $(\Delta t)_{min}$ that could be observed in the image is therefore

$$(\Delta t)_{min} = -\frac{1}{Q} \ln \left[1 - \left(\frac{\Delta I}{I}\right)_{min}\right] \qquad (li)$$

$$\backsimeq \frac{0.05}{Q} = \frac{.05\ M}{N_o \sigma_{atom} \rho}$$

The greater the density ρ, and the total cross-section per atom, σ_{atom}, the higher is the sensitivity to thickness variations. For example, platinum has a value for $Q = 64.5 \times 10^4$ cm^{-1} (47). The minimum thickness that can be observed when platinum is used as the shadowing material is

$$(\Delta t)_{min} = \frac{.05}{64.5 \times 10^4} \simeq 8 \text{ Å}$$

Design of the decoration replica:

The design of the decoration replica should take into consideration the amount of gold and carbon to be evaporated in order to arrive at optimum thicknesses of these elements on the surface. For this purpose, the distance between the specimen and the source of evaporation is to be fixed. To avoid unduly heating the surface of the specimen when gold and carbon are evaporated, this distance is fixed to be 10 cm. If the material that is evaporated from the filament is spherically distributed, an assumption that is valid when a thin wire of gold is evaporated from a tungsten filament, the weight of material M (in grams) required to lay down a deposit of thickness t (in cms), perpendicularly onto the surface at a distance r (in cms), can be calculated from the expression (40)

$$M = \frac{16\pi}{3} \times t \times \rho \times r^2$$

Thickness of gold layer required on the surface for decoration t $= 10 \times 10^{-8}$ cm. The density of gold = 19.3 g/cm^3. Therefore

Amount of gold to be evaporated $= \frac{16\pi}{3} \times 10 \times 10^{-8} \times 19.3 \times 10^2 = 3.01$ mg.

Gold used for evaporation is in the form of a wire of diameter .02 cm.

Length of wire needed for evaporation $= \frac{3.01 \times 10^{-3} \times 10}{\pi \times 10^{-2} \times 10^{-2} \times 19.3} = 5$ mm

A similar calculation can be made to estimate the amount of carbon necessary for the formation of a supporting layer of thickness 100 Å.

$$\rho \text{ for carbon} = 2.3 \text{ g/cm}^3$$

Amount of carbon necessary for the formation of the supporting layer

$$= \frac{16\pi}{3} \times 100 \times 10^{-8} \times 2.3 \times 10^{2} = 4 \text{ mg}$$

Features of platinum-carbon replica:

Platinum-carbon pellets obtained from the Ladd Research Industries, Burlington, Vermont, have been used for the formation of these replicas. They have a composition of 50% (by weight) platinum and 50% (by weight) carbon. The self shadowing technique is employed in replicating the surfaces in which platinum and carbon are simultaneously deposited by evaporating the platinum-carbon pellets.

The replicas should have a thickness of 100-150 Å for mechanical strength. The design for the replica should take into account the critical thickness for single scattering, the variation in the rates for evaporation of platinum and carbon and the contrast that can be obtained when the shadowing is carried out. The shadowing angle is fixed as 30° so that a step of height h casts a shadow of length $\sqrt{3}h$. This shadowing angle is chosen for the reason that at angles less than this a heavy deposit is formed on elevations projecting from the surface (for example, if the angle is 15°, the deposit on elevations is about 500 Å) at the cost of resolution; higher angles of shadowing reduce the length of the shadow cast by the steps, thereby rendering the detection of very fine steps difficult.

The scattering cross-section for platinum Q is 64.5×10^4 cm^{-1} and that for carbon is 8×10^4 cm^{-1} (47). The condition for single scattering in platinum film is

$$t_{critical} = \frac{1}{64.5 \times 10^4} = 155 \text{ Å}$$

Critical mass thickness for platinum = $\rho t = 21.45 \times 155 \times 10^{-8}$

$= 3.325 \times 10^{-5}$ g/cm^2.

Critical thickness for single scattering in carbon films is

$$t_{critical\ (carbon)} = \frac{1}{8 \times 10^4} = 1250 \text{ Å}$$

Hence in dealing with platinum-carbon films of thickness 100-150 Å, the assumption that there is only single scattering in these films is valid.

The slopes of the etch pits in lithium fluoride have been measured by Ives and Hirth (20) to vary between 5-12° depending on the etching conditions. For the sake of simplicity in understanding how contrast arises in the self-shadowed replicas, an etch pit with only one step is shown in Figure 8.

In view of the fact that metal atoms do not exhibit any appreciable mobility, it can be assumed that no platinum is present in the shadowed region. Since carbon atoms migrate appreciably they will be more or less uniformly distributed in all the regions in the pit. Even though the starting mixture is 50% platinum and 50% carbon (by weight), the composition of the deposit on the surface may be different for two reasons:

(a) the evaporation rates of platinum and carbon are not the same, and

(b) carbon atoms have a much greater surface mobility than platinum atoms.

The net vaporisation flux, J_v, for an evaporating material at a pressure P is given by (48)

$$J_v = \frac{\alpha_v (p_e - p)}{(2\pi mkT)^{1/2}}$$

where p_e is the equilibrium vapour pressure at temperature T, m the molecular mass of the material, k the Boltzmann constant, and α_v* the evaporation coefficient. To calculate the exact values for the vaporisation fluxes, it is necessary to know the values of α_v. p_e and p. If the variation of the evaporation rate due to the difference in mass alone is considered, then the net vaporisation fluxes will be proportional to the square root of the masses. Since the atomic weights of platinum and carbon are 195.1 and 12, respectively, their relative rates of vaporisation are in the ratio of about 1:4. Some of the carbon atoms will move towards the shadowed regions reducing the carbon content in the platinum-carbon films. If the movement of these carbon atoms is neglected, then the scattering cross-section for the composite film will be

$$Q = \left\{ \left(\frac{64.5}{5}\right) + \left(\frac{4}{5} \times 8\right) \right\} 10^4 = 19.3 \times 10^4 \text{ cm}^{-1}$$

This will be the minimum value for Q; as carbon atoms diffuse to the shadowed regions, the value of Q will increase.

The contrast between the shadowed region and the region with the

---

* From the kinetic theory of gases, the net rate of vaporisation is deduced as

$$J_v = (p_e - p)/2\pi mkT)^{1/2}$$

Deviations from the ideal equation are accounted for by the introduction of the vaporisation coefficient, α_v, the value for which varies with the constraints in the system. For large perfect crystals $\alpha_v = 2/3(p/p_e) + 1/3$.(15)

deposit is given by

$$\frac{\Delta I}{I} = Q\Delta t = 150 \times 10^{-8} \times 19.3 \times 10^{4} = 0.29$$

which can be easily detected. The contrast will be slightly more than this value since the minimum value for Q is taken into consideration in this calculation.

Since the incident beam of evaporating material does not cast any shadow on the other side of the pit, the contrast here is different. For a shadowing angle of 30°, the thickness of the deposit on vertical and horizontal regions will be in the ratio of cos 30:sin 30, i.e. $\sqrt{3}$:1. If the thickness on the horizontal region is 150 Å, then the film thickness in the vertical region is $\sqrt{3}.150$ Å. The minimum contrast between the horizontal and vertical regions is

$$\frac{\Delta I}{I} = 150 \times .732 \times 19.3 \times 10^{4} \times 10^{-8} = .21$$

which can easily be detected.

It should be stressed that these calculations are empirical but they do help to show that there is a good contrast between the shadowed and unshadowed regions.

Experimental Procedure:

Etching of lithium fluoride: The crystals of lithium fluroide used in this work were purchased from the Harshaw Chemical Company, Cleveland, Ohio. Thin specimens of thickness 1 mm were made by cleavage across {100} planes of the crystals. Good cleavages were obtained with a steel chisel tapped sharply but lightly with a hammer.

The etchant was made by initially preparing a stock solution containing 1500 p.p.m. of Fe; for this purpose 7.26 g of $FeCl_3.6H_2O$ was dissolved in 1 litre of water and a few drops of hydrocloric acid were added to suppress the precipitation of $Fe(OH)_3$. From this stock solution (p_H 2.8) a series of solutions, with the concentration of iron ranging from 0.30 p.p.m. to 150 p.p.m., was prepared.

In all the etching experiments the matching cleavage faces were also etched. One piece was then employed for examination with the interference microscope and the other for the preparation of the replica for electron microscopic examination.

In order to obtain sufficient information regarding the dissolution of lithium fluoride in water in the presence of ferric ion inhibitor, the formation of etch pits was studied at a number of concentrations of iron, viz. 0.3, 1.5, 3.0, 6.0, 9.0, 15, 30, 60 and 150 p.p.m. The time of etching was also varied ranging from an instantaneous etch obtained by dipping the specimen momentarily into the etchant and withdrawing it, to 2 minutes.

A standard immersion procedure was adopted for all experiments in which the etching time was 30 seconds or 2 minutes. Samples were held in teflon covered tweezers and turned by a clock motor in a circle of 3 cm diameter at 60 r.p.m. A typical etchant bath consisted of 25 ml of solution contained in a 50 ml glass beaker. For short time etches (instantaneous, 5 second and 10 second etches), hand stirring was employed.

The specimens, after they were etched, were removed and washed by agitation in absolute alcohol (15 seconds), followed by a short rinse in anhydrous ether (15 seconds). Both rinse baths were continually renewed to avoid contamination. After the ether wash, the samples were dried by a

hot air blower. The need for washing stems primarily from the need to remove excess solution from the sample.

The etched surfaces were examined with a Zeiss interference microscope and the interference patterns were obtained by illumination with thallium light ($\lambda = 0.54\mu$). The patterns were recorded on Eastman Kodak Panatomic-X 35 mm film. The interference micrographs obtained with inhibitor concentrations 0.3, 1.5, 3, 15 and 150 p.p.m. Fe for an etching time of 2 minutes are presented in Figure 7 (a to e).

Decoration technique:

Both as-cleaved and etched samples of lithium fluoride were used as substrates for the nucleation of gold. The evaporation of gold and carbon was carried out in a 'Speedivac' coating unit where a vacuum of better than 1×10^{-5} mm Hg was obtained. The vacuum dropped to about 5×10^{-5} mm Hg when the elements were evaporated.

The sample was held on a molybdenum boat which could be heated by passing current through it. The temperature of the boat could be varied by varying the current. Gold in the form of a wire .02 cm diameter was evaporated from a tungsten filament. The experimental set up is shown in Figure 9. Before the beginning of every experiment, the molybdenum boat and tungsten filament were heated to white heat in a vacuum of 1×10^{-5} mm Hg to remove any foreign material sticking to them.

The etched surface was placed on the molybdenum boat and evacuation of the vacuum unit was started. When the vacuum reached 1×10^{-5} mm Hg, the boat was heated to the desired temperature. Temperatures of 100°, 200° and 300°C were tried with the cleaved specimens while with etched specimens

temperatures in the range 100°-600°C were tried.

The evaporation of gold was carried out only after a vacuum of less than 1×10^{-5} mm Hg had been maintained for at least an hour and the specimen heated for at least 30 minutes. The evaporation of carbon was carried out by striking an arc between two carbon electrodes. No attempts were made to measure the amount of carbon evaporated. The optimum thickness of the carbon film was found by trial and error and the time of evaporation of carbon was controlled to form films of this thickness.

After evaporation, the vacuum unit was cooled and the specimen removed. Stripping of the films was, at first, carried out by lowering the specimen gently into water; occasionally the films could very readily be removed but in many cases they could not be stripped even after allowing the specimen to sit in water for more than a day. There was an interesting observation made with films stripped in water; most of the films, when examined in the electron microscope, were found to carry along with them a thin layer of lithium fluoride. The fact that this was lithium fluoride was established by taking electron diffraction patterns. The layer of lithium fluoride volatilised spontaneously while under observation in the microscope, owing to bombardment by electrons. In order to avoid removing a layer of lithium fluoride along with the decoration replica, a 1N solution of hydrochloric acid (in which lithium fluoride is more soluble) was employed to strip the replicas. The stripped films were subsequently transferred to a distilled water bath; using a sharp pit, they were cut into small pieces. These were picked out on 200 mesh copper grids, dried and used for electron microscopic examination.

Reproducible decoration patterns could be obtained on cleaved surfaces of lithium fluoride, but with etched surfaces it was found that, irrespective of surface temperature, there was only random nucleation of gold on the surface and no obvious decoration effect.

The Self-shadowed platinum-carbon replicas:

Self-shadowed platinum-carbon replicas of the as-cleaved and etched surfaces of lithium fluoride were made by evaporating platinum-carbon pellets at an angle to the surface in a high vacuum unit. The platinum-carbon pellets had a composition of 50% Pt and 50% C (by weight); they had an average diameter of .15 cm. The pellets were introduced in a cylindrical hole drilled in carbon rods.

The etched specimens were lightly cemented to a glass slide by using formvar solution and the slide was fixed in a slotted arm that was free to rotate about a horizontal axis on a pivot with an attached protractor. The slide could be secured at any desired angle with a screw. The whole assembly could be moved up and down on a vertical rod and in this way the distance of the specimen from the source of evaporation could be adjusted. This distance was kept at 10 cms in all the experiments. Care was taken to see that vacuum of a high order was maintained before the pellets were evaporated. After evaporation, the vacuum chamber was cooled and the specimen removed from the glass slide. The replicas were stripped using 1N hydrochloric acid solution, washed with distilled water, picked out on 200 mesh copper grids, dried and then examined in the electron microscope. The replicas were examined in the Siemens Elmiskop I electron microscope.

Precautions to be taken in using shadowing technique:

The main requirement for the formation of sharp shadows is the establishment of a sufficiently high vacuum before evaporating the metal. Granulation of the deposit occurs if the vacuum is not good enough. If the vacuum is so poor that the mean free path of electrons is less than the specimen-source distance, the shadows themselves will lose sharpness. If granulation is to be kept to a minimum, vacuum of the order of 10^{-4} to 10^{-5} mm Hg is necessary and this must be maintained for at least an hour to avoid a large burst of gas due to the heating effect of the filament when evaporation is started (36).

It is necessary to keep down the beam current of the electrons in the electron microscope to a minimum since too high a current also brings about granulation even if this has been avoided in the process of evaporation. If the advantage gained by long evacuation before evaporation is not to be wasted, the lowest beam current should be employed at which adequate examination of the specimen can be made.

As has been pointed out before, contrast in these replicas is dictated by thickness variations and scattering cross-section for the electrons by the object. Since the latter decreases with increase in accelerating voltage for the electrons, it is preferable to use an accelerating voltage of 40 or 60 kV when examining these replicas in the electron microscope. In this work an accelerating voltage of 60 kV was employed.

Artifacts and defects in replicas:

Artifacts can be defined as structures which are not germane to the investigation and which may actually interfere with obtaining a satisfactory

interpretation of the image. Because replicas are a substitute for an actual surface, artifacts are more common and in fact their recognition is almost synonymous with correct interpretation of electron micrographs. Wrinkles, bumps and pockets observed in thick plastic film intermediate replicas are some examples of artifacts. There are other examples like dust particles, unwanted surface films and residues from chemical etches. Granularity due to plastic molecules and that due to crystallinity are common occurrences.

Results:

The decoration patterns obtained on cleaved surfaces of lithium fluoride are shown in Figures 10 and 11. As has been pointed out earlier, no discernible decoration pattern was obtained on etched surfaces.

The electron micrographs of the replicas of surfaces of lithium fluoride subjected to varying etching conditions are shown in Figures 12 to 43.

CHAPTER IV

INTERPRETATION OF RESULTS AND DISCUSSION

The decoration replicas:

The decoration patterns obtained on cleaved surfaces of lithium fluoride at substrate temperatures of 200° and 300°C are shown in Figures 10 and 11.

It is clearly seen in both the micrographs that the density of gold nuclei along the steps is much more than what it is in other regions. The individual steps seen in Figure 11 are considerably kinked as can be followed by the wavy nature of arrangement of the gold nuclei. Small rectangles formed by gold nuclei probably correspond to pits formed by the localised evaporation of lithium fluoride. In both the figures steps containing right angle bends are clearly seen. A similar observation on the cleavage surfaces of sodium chloride has been explained (34) as evidence for cross-slip. Sodium chloride and lithium fluoride have similar slip systems and hence it is possible that cross-slip occurs in lithium fluoride also. Gilman and Johnston (49) have found that screw dislocations can cross-glide onto {100} planes. The cross-glide of screw dislocations often occurs in the vicinity of glide bands where there is a sharp gradient in plastic strain. The dark region seen on the left hand side of Figure 10 is a fold in the replica.

Bassett (34) has measured the heights of the individual steps by determining the displacement suffered by a slip step when it crosses a

stair case of cleavage steps; since it is not possible to detect any slip step crossing the cleavage steps, the height of the steps decorated by gold nuclei cannot be established.

The preferential nucleation of gold along the steps can be easily understood by considering the rate of nucleation. The calculation of the nucleation rate is carried out in three stages (50):

(a) the concentration of the critical nucleus is determined,

(b) the nucleation rate is given by the product of the concentration of the critical nuclei and the rate of impingement of single molecules, and

(c) a correction is applied, the Zeldovich factor, which takes into account the departure from equilibrium due to nucleation and the fact that some of the nuclei that have transformed through the accretion of a single molecule can lose that molecule and revert to nuclei. The Zeldovich factor is usually not large and is neglected (50).

By assuming that the shape of the critical nucleus is constant and spherical, and bulk thermodynamic quantities can be used in computing the free energy of formation of the critical nucleus, Pound, Sinmad and Yang (50) have shown that the nucleation rate, I, is

$$I = \frac{4\pi\gamma \sin \quad Ra_o N_o}{\Delta G_v} \exp\left[\left(\frac{Q_{ad} - Q_D - \Delta F^*}{kT}\right)\right] \qquad \text{(lii)}$$

where γ is the surface energy, the substrate-deposit contact angle, a_o the separation between adsorption sites, N_o the number of adsorption sites per unit area of the substrate surface, Q_{ad} binding energy of a single atom to the surface, Q_D the activation energy for diffusion, ΔF^* the free energy of formation of the critical nucleus, and $\Delta G_v = kT \ln p/p_e$ where p_e is the vapour pressure of the deposit at substrate temperature.

The use of the bulk value for surface energy in computing the free energies of small clusters has been criticised on the grounds that the definition of this quantity is ambiguous for small groups of atoms. For very small groups the assumption of an invariant structure is also inadequate.

Walton (51) has employed a statistical mechanical approach to calculate the concentration of the critical nucleus. The nucleation rate, I, according to this approach, is

$$I = Ra_o^2 N_o \left(\frac{R}{\nu N_o}\right)^{n^*} \exp\left[\frac{(n^* + 1)\, Q_{ad} + E_{n^*} - Q_D}{kT}\right] \quad \text{(liii)}$$

where n^* is the number of atoms in the critical nucleus and E_{n^*} the energy required to dissociate the cluster into n single atoms.

Rhodin and Walton (51) have shown that the nucleation rate on steps, I', is given by

$$I' = R\left(\frac{R}{\nu N_1}\right)^{n^*} \exp\left\{\frac{\left[(n^* + 1)\, Q_{ad} + E_{n^*} - Q_D + Q_{n^*} + Q_1\right]}{kT}\right\} \quad \text{(liv)}$$

where Q_{n^*} is the binding energy of the critical nucleus to the step and Q_1 the binding energy of a single atom to the step.

It is clearly seen that the nucleation rate on the steps (I') is simply the nucleation rate on the surface (I) multiplied by $\exp\,(Q_{n^*} + Q_1)/kT$. Since Q_{n^*} at the very least is equal to Q_1, the nucleation rate is (very approximately) higher by a factor $\exp\,(2Q_{ad})/kT$. The above equations hold good only when there is no adsorbed layer on the surface. Surfaces of lithium fluoride, when etched in the 'W' etchant, adsorb impurities. When an adsorbed layer is formed, the nucleation

characteristics are controlled by the nature of the adsorbed layer and no longer by the substrate. This is probably the reason for the random nucleation of gold on etched samples of lithium fluoride.

Self-shadowed platinum-carbon replicas:

The self-shadowed replica of the as-cleaved surface of lithium fluoride (Figure 12) reveals a number of cleavage steps of heights ranging from 80 to 135 Å. Some faint steps of height 30 Å and a few appreciably kinked macrosteps are also seen.

These cleavage steps are formed by the intersection of the propagating cleavage crack with screw dislocations. The dislocations giving rise to the cleavage steps can originate in three ways:

(a) they can be grown into crystals,

(b) they can be introduced by plastic deformation prior to cleavage, and

(c) they can be formed just in front of the tip of a propagating crack.

Gilman (52) has employed the technique of cleaving pre-strained crystals of lithium fluoride and subsequent etching to prove that cleavage steps are formed only at the screw dislocations while edge dislocations have no effect.

Dislocation loops are nucleated by slowly moving cracks just in front of the crack tip (53). These loops lie on {110} planes. The screw components of the dislocation loops are severed when the advancing crack cuts through the loops and cleavage steps are left behind. The paths followed by the cleavage steps depend on the angle between the crack front and the dislocation loop that produces the step.

The profound changes in dissolution morphology brought about by etching in distilled water for 30 seconds is shown in Figure 13. A comparison

of Figure 12 with Figure 13 suggests that the long mainly unkinked macrosteps formed during cleavage are rendered unstable; they are replaced by considerably kinked macrosteps. A number of nuclei is seen but there is no suggestion for the development of well defined etch pits.

The observation of kinked macrosteps and nuclei can be explained as follows: Lithium fluoride is moderately soluble in water (0.27 g/100 ml of water at 18°C). Therefore when a crystal of lithium fluoride is introduced in water, because of finite undersaturation, dissolution begins. As has been pointed out earlier, dissolution starts preferentially at the sites which act as sources for ledges, viz. dislocations, point defects and crystal corners. If there are no impurities in water, the kinks formed in the ledges will strip the latter rapidly thereby resulting in smooth ledge features. But the presence of only trace impurities which can cause effective inhibition by adsorption at some of the kink sites can stabilise kinked ledges. Also impurity adsorption lowers the velocity of a ledge thereby giving a chance for the following ledges to catch up with the poisoned ledge. The result of this is the formation of a bunched macroscopic ledge. The height of the bunched ledge is controlled by the number of individual ledges that have joined together to form the macroledge.

Since even trace impurities present in distilled water are able to stabilise kinks and since it is known that Al^{+++} and Fe^{+++} are the effective inhibitors (28), it is possible to offset their effect by the addition of ammonium hydroxide to the solution when the impurities are precipitated. The solubility product of ferric hydroxide is 1.1×10^{-36} (at 18°C) (54) and therefore in dealing with solutions of water containing small amounts of ammonium hydroxide the concentration of iron is extremely small. Based

on this principle, Gilman and Johnston (30) have developed a polishing agent for lithium fluoride containing 1.5% concentrated ammonium hydroxide in distilled water.

Figures 14 and 15 show the changes in etch features brought about by the polishing solution. A striking feature is the absence of kinked macroledges. A number of nuclei is seen on the surface but it is difficult to reveal the structure inside the nuclei. The small amount of kinked ledges on the surface indicates that ammonium hydroxide forms precipitates with the inhibitor ions rendering them ineffective.

The gradual addition of iron to the etching solution facilitates the formation of etch pits and the changes in etch features brought about by varying concentration of iron are shown in Figures 16 to 29.

The etch features observed by the instantaneous etching of lithium fluoride (Figure 16) are similar to those observed in the distilled water etch for 30 seconds; a high density of kinked macrosteps due to bunching is seen but the density of nuclei in this case is less than that with the distilled water etch.

Ives and Hirth (20) have explained the formation of etch features on lithium fluoride in the presence of iron inhibitor by assuming a time-dependent adsorption of the inhibitor. If this is the case, starting with two slightly different concentrations of iron, it should be possible to produce similar etch features by varying the time of etch suitably. The fact that the specimens etched with distilled water for 30 seconds (containing traces of iron) and 0.3 p.p.m. iron etch (instantaneous etch) reveal more or less the same features indicates in a qualitative way that the explanation based on time-dependent adsorption is satisfactory.

When the time of etching is increased to 30 seconds, there is a tendency for the formation of etch pits as revealed in Figure 17. The pits are flat-bottomed and at the edges the density of ledges is considerable. A few spirals formed by dissolution are feintly visible. The ledges observed are all kinked.

An examination of the specimens, etched with water containing 0.3 p.p.m. iron, by optical and interference microscopy, shows kinked ledges and rough surface features but no etch pits. Autoradiography (33) has revealed that corresponding to this concentration of iron, the adsorption is extremely low. Only when the concentration of iron reaches 2 to 3 p.p.m. does the adsorption correspond to monokink coverage.

The effect of increasing the concentration of iron, to near the optimum concentration, on the etch features is shown in Figures 18 and 19. Instantaneous etching of surfaces of lithium fluoride in etchant containing 1.5 p.p.m. iron reveals well defined etch pits many of which are pyramidal and pointed, while a few are flat-bottomed. Some of the pointed etch pits are symmetric about the centre while the others are asymmetric. The kinked ledges are still observed but are extremely fine.

The formation of pyramidal pits, both pointed and truncated, can be explained on the basis of the difference in the velocities of the ledges and nucleation at the dislocation. If the velocity normal to the surface is v_n and that of the ledges is v_s, when v_n is considerably smaller than v_s very shallow pits will be formed. It has been found (28) that when $v_n/v_s \geq 0.1$, readily visible pits can be formed. When v_n is considerably smaller than v_s (an effect that can be brought about by a very low nucleation rate or by ineffective inhibition), the pits produced are truncated.

The dissolution of lithium fluoride in water in the presence of iron inhibitor gives rise to pointed pyramidal pits at dislocation sites, while with polar molecules the pits formed are flat-bottomed. If a dislocation has moved during the process of etching or if the nucleation rate is lowered (due to reduction in core energy of the dislocation or nucleation at point defects becoming negligible), v_n becomes small and flat-bottomed pits are produced.

Figure 19 shows the regular etch pits formed when the etching time is increased to 30 seconds. The ledges in the pits are uniformly spaced but their height is more than that observed with the macroledges obtained by instantaneous etch (Figure 18). This seems to indicate that the effect of bunching increases with time. Some dissolution spirals and a bunch of kinked ledges are also seen. The wavy nature of the ledges in the pits suggests that kinks are considerably stabilised.

The change in etch features brought about by the presence of more than the optimum concentration of iron is shown in Figures 20 and 21 where a concentration of 6 p.p.m. iron is used. Instantaneous etching of the specimen produces well defined etch pits, some of which are flat-bottomed and others pointed, Kinked and bunched ledges are also seen. The areas enclosed by small dark circles are artifacts possibly due to impurities on the surface. When the etching time is increased to 30 seconds, the pits become deeper and the ledges constituting the pits become finer (Figure 21). Some flat-bottomed pits are also seen. The individual ledges in the pits contain large quantities of stabilised kinks.

Figures 22 and 23 reveal the etch features obtained with an inhibitor concentration of 15 p.p.m. iron. The interference micrograph (Figure 7d)

corresponding to this concentration shows etch pits which have started rounding at the edges. The instantaneously etched specimen (Figure 22) contains a number of pits with square ledges at the centre. The edges of the pits are rounded. The attack on the surface is very rough. The specimen etched for 30 seconds shows that the ledges constituting the pit are fine (Figure 23). The ledges are square at the centre but they are irregular at the edges indicating that there is a tremendous amount of kink stabilisation. A pit at the top is almost rounded at the edges. Two pairs of pits are seen at the right hand side of the micrograph. Gilman and Johnston (49) have shown that pairs of pits formed by etching correspond to dislocation half loops. Dislocation half loops of two kinds have been observed in lithium fluoride (49). For one type of loop the dislocations that intersect the surface are parallel to the Burgers vector and are therefore screw dislocations. For the other type the dislocations that intersect the surface lie perpendicular to the Burgers vector, i.e. they are edge dislocations. The loops intersecting the $\{100\}$ cleaved surfaces of lithium fluoride are schematically shown in Figure 43.

The etch pits seen at the lower right hand corner of the micrograph (Figure 23) have their line of centres inclined at 45^{o} to a $\langle 100 \rangle$ direction and are therefore formed from a half loop with 2 edge components. The $\langle 100 \rangle$ direction is fixed from the fact that the edges of the pits are parallel to this direction. The line of centres of the other pairs is slightly inclined to a $\langle 100 \rangle$ direction. This indicates that one of the dislocations has either climbed or cross-slipped.

The interference micrographs reveal that when the concentration of iron is more than about 20 p.p.m. the pits become quite rounded (Figure 7e).

Electron micrograph (Figure 24) of an instantaneously etched specimen with an inhibitor concentration of 30 p.p.m. iron reveals pits which are square at the centre but rounded at the edges. In addition, a few rounded and flat-bottomed pits are seen. Increasing the time of etching to 30 seconds produces pits with square ledges at the centre but irregular at the edges (Figure 25).

It is seen that with high concentrations of iron ($>$ 15 p.p.m.) the pits become smooth and it is very difficult to resolve the individual ledges in the pit.

There is no significant change in the morphologies observed with higher concentrations of iron. Instantaneous etching produces pits with square ledges at the centre and rounded at the edges while a 30 second etch produces very smooth pits (Figures 26, 27, 28 and 29). The ledge structure is so smooth that when the inhibitor concentration is 150 p.p.m. iron the self-shadowing technique forms replicas which show no contrast between the ledges inside the pits. Pre-shadowed gold replicas were used to show the resolution of the ledges to some extent (Figure 29) (55).

The development of pits of different shapes at edge and screw dislocations is well brought about in Figure 30 showing the surface of lithium fluoride etched with 1.5 p.p.m. iron for two minutes. Most of the pits observed are asymmetric about the centre while a symmetric pit and some dissolution spirals are also revealed.

The orientation of the dislocation with respect to the surface can be inferred from the shape of the pit. The line drawn from the centre of the base of the pyramidal pit to the apex of the pyramid will be tangent to the dislocation line (56). Taking into consideration the fact that edge

dislocations emerge at glide bands lying in $\langle 110 \rangle$ directions and screw dislocations at glide bands lying in $\langle 100 \rangle$ directions, it is easy to see that on the $\{100\}$ cleavage planes edge dislocations from symmetrical etch pits and screw or mixed dislocations give rise to asymmetric etch pits. This is schematically represented in Figure 44.

Very often it is possible to reveal the dislocations present in deformation bands by etching. The nature of the dislocations present in the band can be very easily established by taking into account the orientation of the band.

Figure 32 reveals the dislocations present in a band through the formation of etch pits with an etchant concentration of 3 p.p.m. Fe, the etch time being 30 seconds. The band is parallel to the edges of the pits. Therefore the individual dislocations in the band must have screw character. Dislocation band consisting of edge dislocations is clearly revealed in Figure 33. In this case the band is inclined at an angle of 45° to the edges of the pits.

It is interesting to note that even with higher concentrations of iron the etch pits formed at the glide bands retain their pyramidal nature. Figures 34 and 35 illustrate this effect, the etchant containing 9 p.p.m. iron and the etch time being 30 seconds and 2 minutes, respectively. The glide band in Figure 34 is parallel to the edges of the pits and the individual dislocations have therefore screw character. The presence of half loops is indicated by pairs of pits. On the other hand, the dislocations present in the band in Figure 35 have edge character.

Both screw and edge bands are revealed in Figure 36. Edge dislocations lie along the horizontal and vertical lines while the lines of

screw dislocations are inclined at 45°. It is interesting to note that this micrograph compares very well with optical micrographs obtained with an etch time of two minutes.

Occasionally it is found that the attack on the surface is considerable. An example of this is shown in Figure 38 where the etch features on a surface of lithium fluoride etched with 9 p.p.m. iron for two minutes are seen. The nucleation density is very high and the size of the pits varies considerably. Pairs of pits corresponding to dislocation half loops and some flat-bottomed pits are also seen. This type of attack is not very frequently seen and is probably associated with etching of impurity sites in addition to the dislocations.

A complete examination of the electron micrographs suggests that the following points merit serious consideration:

The pits are flat-bottomed at the lowest concentration of iron and with increasing inhibitor concentration they become pyramidal; with low concentration of iron, ledges are stabilised towards the edge of the pits. The heights of the ledges in the pit decrease with increasing concentration of iron. In other words the tendency for bunching becomes less pronounced with an increase in the inhibitor concentration. The pits have square sections at the centre irrespective of the concentration of iron. The edges are rounded at short etch times for high concentrations of iron while they are irregular at longer times.

No quantitative treatment of the various possibilities of partial or complete adsorption poisoning at kinks or at ledges is available and as such the results obtained can be interpreted only in a qualitative manner.

The adsorption of iron at the surface reduces the surface energy. At the same time there is a decrease in the solubility of lithium fluoride. Since the latter is a less marked effect than the former, it is to be expected that the activation energy for two dimensional nucleation on a perfect surface will be lowered by the adsorption of inhibitor.

The activation energy for nucleation at a dislocation site, ΔG, is given by

$$\Delta G = - \frac{\pi \gamma^2 \Omega h}{kT \ln c/c_o} - h E(r)$$

A reduction in the surface energy lowers the activation energy for nucleation at a dislocation (if the strain energy of the dislocation is not affected by the adsorption of the inhibitor). Westwood et al. (31) have found that the etch pits formed at dislocation sites on the surface of lithium fluoride are flat-bottomed when long chain fatty acids are used as inhibitors; in addition the growth rate of the pits is considerably reduced. To explain these observations, Westwood et al. (31) have suggested that the adsorption of inhibitor at the core of the dislocation lowers the core energy. If this is the case then the activation energy for nucleation will be controlled by the reduction in surface energy due to adsorption of the inhibitor on the surface and the reduction in core energy of the dislocation.

Gilman and Johnston (49) have found that the rate of dissolution of a freshly cleaved surface of lithium fluoride in water is almost equal to that at the centre of the pits formed in water with iron as the inhibitor. This rules out the possibility of reduction of core energy by the adsorption of inhibitor (if adsorption of inhibitor at the core of the dislocation reduces the core energy, then the dissolution rate at the centre of the

pit will be less than that with surfaces in water).

The formation of flat-bottomed pits can, therefore, be explained only on the basis of ineffective inhibitor control of ledges after they leave the dislocation site. Adsorption studies on the surfaces of lithium fluoride dissolving in water in the presence of iron (33) have revealed that the kink sites in the ledges are effectively inhibited only when the concentration of iron is 2 to 3 p.p.m. At concentrations considerably lower than this, the amount of iron available for inhibition is very low and this results in partial inhibition of the kink sites.

The fact that multi-ledges are stabilised at the edge of the pits while at the centre no ledges are seen (Figure 17) suggests that the concentration of the inhibitor in different regions in the pit is not the same.

A prominent factor which introduces a change in the concentration of iron between the centre and edge of the pit is the lithium fluoride gradient that exists in the pit. Ives and Plewes (57) have shown that the surface dissolution rate of lithium fluoride is markedly affected by the presence of small amounts of iron. It is, therefore, obvious that the dissolution rate at the centre of the pit (where there is no inhibition since an inhibitor can act only after nucleation) is more than that at regions away from the centre of the pit. This produces a gradient in the lithium fluoride concentration in the pit.

The chemical equation for the formation of complexes in solution can be written as

$$nF^- + FeF_3 \rightleftharpoons Fe\,F_{3+n}^{n-}$$

where n can be 1, 2 or 3.

An increase in the value of a_{F^-} favours the reaction to proceed in the forward direction (by the Le Chatelier principle) thereby reducing the equilibrium concentration of iron in solution around the centre of the pit.

Another point of interest is that the inhibitor does not necessarily assert a constant constraint on a particular ledge as it travels outward from the source. For a square (or circular) ledge the rate of increase of ledge per unit length of the complete ledge is inversely proportional to the width (or radius) of the continuous ledge, i.e. dl/l or $dr/r \propto 1/r$ (20).

If the rate of poison accumulation from solution (in atoms/cm^2/sec) is constant, there will be a consequent time dependence of poison at a ledge. For ledges near the dislocation line, the rate of ledge length increase per unit length is very large while at large length this increase is reduced. It is, therefore, probable that the poison cannot inhibit each ledge equally, since there will be some ledges that are increasing in length at too great a rate to allow any effective inhibition, while others are expanding slowly enough for inhibitor to be completely effective. The fact that at the centre of the pit ledges are increasing in length at a rapid rate coupled with the fact that the concentration of iron is very low (0.3 p.p.m.) can account for the observation of flat-bottomed pits. With increasing concentrations of iron the number of ferric ions available for inhibition increases and hence better inhibition is obtained.

It has already been indicated that bunching of the ledges is brought about by adsorption of impurities. The height of the bunched ledge is controlled by the number of ledges catching up with a more slowly moving ledge. In the presence of a large quantity of the inhibitor it is to be expected that a large number of the ledges will be slowed down by the adsorption of

iron. As such the number of individual ledges constituting a bunched macro-ledge will be small.

Also, once the concentration of iron exceeds the optimum concentration (corresponding to the condition of monokink coverage), multi-layer adsorption begins. When this condition is attained the effect due to the inhibitor will be significant. In the limit the ledges will be poisoned immediately they are emitted at the source. The time dependence of poisoning will then no longer exist. The shapes of etch features obtained in this case will be governed by the rate of nucleation. If the nucleation rate is only moderate (as is the case with lithium fluoride in water), the few stabilised kinks in the ledges will not confer any appreciable change in the shape of the pits. In other words, the pits will be made up of very fine ledges with a few stabilised kinks.

Dissolution spirals:

The formation of spirals during the inhibited dissolution of lithium fluoride is clearly revealed in Figures 39, 40, 41 and 42, and to a limited extent in Figures 17, 19, 30, 31 and 37. The heights of these spirals vary considerably ranging from 75 Å to 200 Å. The spirals have been observed under varying etching conditions. However, spirals were never observed when the concentration of iron exceeded 10 p.p.m.

When a screw dislocation ends at the surface it produces a step. Growth or dissolution at a screw dislocation site proceeds by the addition or removal of atoms resulting in the formation of growth or dissolution spirals. The step height of the spiral is equal to the component of the Burgers vector of the dislocation normal to the surface. On the basis of

this simple idea the spirals observed on the surfaces of lithium fluoride can be explained as being due to screw dislocations with Burgers vectors in the range 75 to 200 Å (about 20 to 50 times the lattice parameter of lithium fluoride).

In this connection it is interesting to note that dissolution spirals with step heights of 1000 Å have been observed in the etching of germanium and silicon. Christian and Jensen (58) have noticed dissolution spirals with step heights of 10^4 - 10^5 Å when silicon was etched with a modified CP-4 reagent. Ellis (59) has reported the observation of etch pits with spiral terraces in germanium. He has ascribed their formation to screw dislocations with Burgers vector of the order of 1000 Å. The formation of screw dislocations with such large Burgers vector has been related to non-uniform temperature gradients and impurity contents causing a mistake in the formation of dendrites. However, this view is no longer held. It is also doubtful whether dislocations of large Burgers vector can be present in lithium fluoride in view of the ionic bonding in the crystal.

Lang (60) has suggested that these spirals are formed when the rate of etching is asymmetric about the point in the surface at which the attack is nucleated. The surfaces of the etch pits are made up of a number of ledges and a simple mistake in the early stages of ledge formation will produce a continuous spiral. This theory suggests that the rate of dissolution parallel to the surface is not uniform - a condition which does not hold good in the etching of lithium fluoride and as such it is to be rejected.

The simplest and most elegant explanation for the formation of spiral etch pits is offered by Bontinck and Amelinckx (61). They have observed helical dislocations in synthetic crystals of fluorite by heating them to

1100°C in a reducing atmosphere in the presence of silver, when decorated helical patterns were observed. The formation of these helices has been explained as due to the condensation of vacancies on dislocations of mixed character (61).

Weertman (62) has shown that the equilibrium form of a dislocation line acted on by an ordinary stress or a chemical stress produced by a deviation of the vacancy (or interstitial) concentration from the equilibrium value is a helix of axis parallel to the Burgers vector and wound around a cylinder of revolution.

When the axis of the helix is perpendicular to the surface of etching, the etch pit formed will, at every moment, be centred on the dislocation line and penetrate in depth at a constant speed. Viewed from above this means that the centre of the etch pit describes a circle during etching. The resulting shape of this combined dissolution can roughly be described as a 'helical cone'. The surface of the pit is generated by a circle, lying in a plane parallel to the plane of observation whose radius decreases linearly with depth and whose centre describes the helix. The resulting etch feature is a spiral. This is schematically represented in Figure 45.

The formation of dissolution spirals can be rationalised based on the presence of helical dislocations formed by the condensation of vacancies on screw dislocations during the solidification of lithium fluoride from the melt. The presence of double spirals (Figures 39 to 42) suggests that vacancies have condensed onto the dislocation half loops that are known to be regularly formed during the cleavage of lithium fluoride.

Conclusions:

(1) Nucleation of gold on etched samples of lithium fluoride is quite random; as such the gold decoration technique cannot be employed to study the ledge features in etch pits.

(2) The profound changes brought about by the inhibitor by way of stabilisation of kinks and formation of well defined etch pits are clearly revealed by electron microscopic study.

(3) The spacing and heights of the ledges in the pits depend on the concentration of the inhibitor in the etchant. At concentrations of iron less than 2 p.p.m., the spacing between the ledges is irregular. Local variations in the concentration of iron seem to govern the stabilisation of ledges. As the concentration of the inhibitor is increased, the ledges are arranged in a regular manner and their heights decrease progressively. The effective role played by the inhibitor is clearly indicated by the fact that even an instantaneous etch produces well defined etch pits.

(4) The presence of half loops introduced by deformation is clearly indicated by pairs of etch pits; there is also some evidence for the initiation of dissolution at other imperfections as revealed by a rough attack on some of the surfaces.

(5) With increasing concentration of iron, the edges of the pits exhibit considerably kinked ledges. But the complete rounding of the pits as revealed in optical micrographs is seen only on specimens etched instantaneously and that too only at the edges.

(6) The formation of dissolution spirals with large step heights suggests the presence of helical dislocations formed by the condensation of vacancies on screw or mixed dislocations.

Suggestions for future work:

Further work is to be carried out to prove the existence of helical dislocations in lithium fluoride. A specimen of lithium fluoride can be heated to a temperature near the melting point and cooled rapidly to make the vacancies condense. This will further support the hypothesis that helical dislocations are present.

It is necessary to make an intensive study of similar systems (for example, NaCl-ethyl alcohol-ferric ion inhibitor) to understand the stabilisation of ledges at high concentrations of inhibitor leading to the formation of irregular edges.

The nature of the complex formed by the inhibitor can be established by infrared spectroscopy.

REFERENCES

(1) J. W. Gibbs, "On the Equilibrium of Heterogeneous Substances". Collected works (Longmans, Green and Co., New York, 1928).

(2) G. Wulff, Z. Krist. 34, 449 (1901).

(3) F. C. Frank, "Growth and Perfection of Crystals". Edited by R. H. Doremus, B. W. Roberts and D. Turnbull (John Wiley and Sons, New York, 1958), p. 3.

(4) N. Cabrera, Discussions Faraday Soc. 28, 16 (1959).

(5) W. Kossel, Nach. Ges. Wiss. Gottingen, 135 (1927).

(6) I. N. Stranski, Z. Physik. Chem. 136, 259 (1928), 11, 421 (1931).

(7) W. K. Burton, N. Cabrera and F. C. Frank, Phil. Trans. Roy. Soc. 243A, 299 (1951).

(8) F. C. Frank, Reference (3), p. 411.

(9) N. Cabrera and D. A. Vermilyea, Reference (3), p. 393.

(10) A. A. Chernov, Dokl. Akad. Nauk S.S.R., 117, 983 (1957).

(11) J. Frenkel, J. Phys. U.S.S.R., 9, 392 (1945).

(12) W. K. Burton and N. Cabrera, Discussions Faraday Soc. 5, 33 (1949).

(13) N. Cabrera and M. M. Levine, Phil. Mag. 1, 450 (1956).

(14) J. P. Hirth and G. M. Pound, Acta Met. 5, 649 (1957).

(15) J. P. Hirth and G. M. Pound, J. Chem. Phys. 26, 1216 (1957).

(16) A. H. Cottrell, "Dislocations and Plastic Flow in Crystals" (Oxford University Press, Oxford, 1953), p. 38.

(17) N. Cabrera, M. M. Levine and J. S. Plaskett, Phys. Rev. 96, 1153 (1954).

(18) N. Cabrera, "Semi Conductor Surface Physics". Edited by R. H. Kingston (University of Pennsylvania Press, Philadelphia, 1957), p. 327.

(19) W. G. Johnston, Progress in Ceramic Science, 2, 1 (1962).

(20) M. B. Ives and J. P. Hirth, J. Chem. Phys. 33, 517 (1960).

(21) A. Carlson, Reference (3), p. 421

(22) M. J. Lighthill and J. B. Whitham, Proc. Roy. Soc. 229A, 281, 317 (1955).

(23) F. C. Frank and M. B. Ives, J. Appl. Phys. 31, 1996 (1960).

(24) M. B. Ives, J. Appl. Phys. 32, 1534 (1961).

(25) L. D. Hulett and F. W. Young, J. Phys. Chem. Solids 26, 1287 (1965).

(26) J. P. Hirth, "Metal Surfaces" (American Society for Metals, Ohio, 1963), p. 199.

(27) W. W. Mullins and J. P. Hirth, J. Phys. Chem. Solids 24, 1391 (1963).

(28) J. J. Gilman, W. G. Johnston and G. W. Sears, J. Appl. Phys. 29, 747 (1958).

(29) M. B. Ives, J. Phys. Chem. Solids 24, 275 (1963).

(30) J. J. Gilman and W. G. Johnston, "Dislocation and Mechanical Properties of Crystals" (John Wiley and Sons, New York, 1957), p. 119.

(31) A. R. C. Westwood, H. Oppenheuser, Jr., and D. J. Goldheim, Phil. Mag. 6, 1475 (1961).

(32) G. W. Sears, "Growth and Perfection of Crystals" (John Wiley and Sons, New York, 1958), p. 442.

(33) M. B. Ives and M. S. Baskin, J. Appl. Phys., 36, 2057 (1965).

(34) G. A. Bassett, Phil. Mag. 3, 1042 (1958).

(35) E. M. Mahla and N. A. Nielsen, J. Appl. Phys. 19, 379 (1948).

(36) V. E. Cosslett, "Practical Electron Microscopy" (Butterworth Scientific Publications, London, 1951), p. 227.

(37) R. D. Heidenreich and V. G. Peck, J. Appl. Phys. 14, 23 (1943).

(38) R. D. Heidenreich and C. J. Calbick, "Physical Methods in Chemical Analysis". Edited by W. G. Berl, Vol. 1 (Academic Press, New York and London, 1960), p. 592.

(39) D. E. Bradley, Brit. J. Appl. Phys. 10, 198 (1959).

(40) "Techniques for Electron Microscopy". Edited by D. Kay (Blackwell, Oxford, 1961), p. 122.

(41) G. A. Bassett, J. W. Menter and D. W. Pashley, "Structure and Properties of Thin Films". Edited by C. A. Neugebauer, J. B. Newkirk and D. A. Vermilyca (John Wiley and Sons, New York, 1959), p. 11.

(42) L. Bruck, Ann. Phys. 26, 233 (1936).

(43) R. B. Kehoe, Phil. Mag. 2, 455 (1957).

(44) H. Bethge, Surface Science 3, 33 (1965).

(45) G. R. Hennig, J. Chem. Phys. 40, 2877 (1964).

(46) G. R. Hennig, Science 147, 733 (1965).

(47) R. D. Heidenreich, "Fundamentals of Transmission Electron Microscopy" (Interscience Publishers, New York, 1964), p. 28.

(48) J. P. Hirth and G. M. Pound, "Progress in Materials Science". Edited by B. Chalmers, Vol. II (Pergamon Press, New York, 1963), p. 2.

(49) J. J. Gilman and W. G. Johnston, Solid State Physics 13, 164 (1962).

(50) G. M. Pound, M. Sinmad and L. Yang, J. Chem. Phys. 22, 1215 (1954).

(51) D. Walton, J. Chem. Phys. 37, 2182 (1962); T. N. Rhodin and D. Walton, "Metal Surfaces" (American Society for Metals, Metals Park, Ohio), p. 259.

(52) J. J. Gilman, Trans. A.I.M.E. 212, 310 (1958).

(53) J. J. Gilman, J. Metals 9, 449 (1957).

(54) "Handbook of Chemistry and Physics", 44th edition (The Chemical Rubber Publishing Co., Cleveland, Ohio, 1962), p. 1746.

(55) Reference (36), p. 244.

(56) S. Amelinckx, Phil. Mag. 1, 269 (1956).

(57) M. B. Ives and J, T. Plewes, J. Chem. Phys. 42, 293 (1965).

(58) S. M. Christian and R. V. Jensen, Bull. Am. Phys. Soc. 1, 140 (1956).

(59) S. G. Ellis, J. Appl. Phys. 26, 1140 (1955).

(60) A. R. Lang, J. Appl. Phys. 28, 497 (1957).

(61) S. Amelinckx, W. Bontinck and W. Dekeyser, Phil. Mag. 2, 1264 (1957).

(62) J. Weertman, Phys. Rev. 107, 1259 (1957).

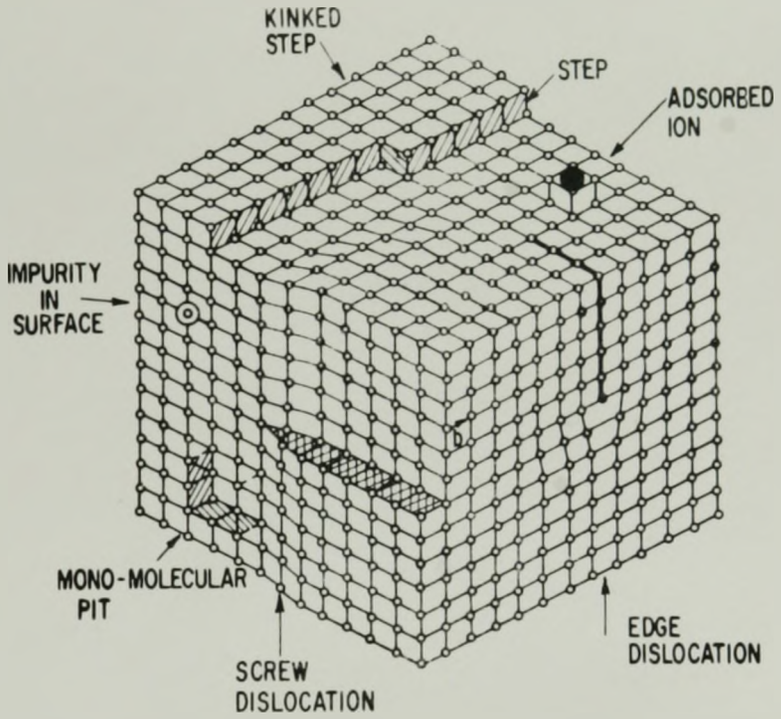

Fig. 1 Surface imperfections on a crystal.

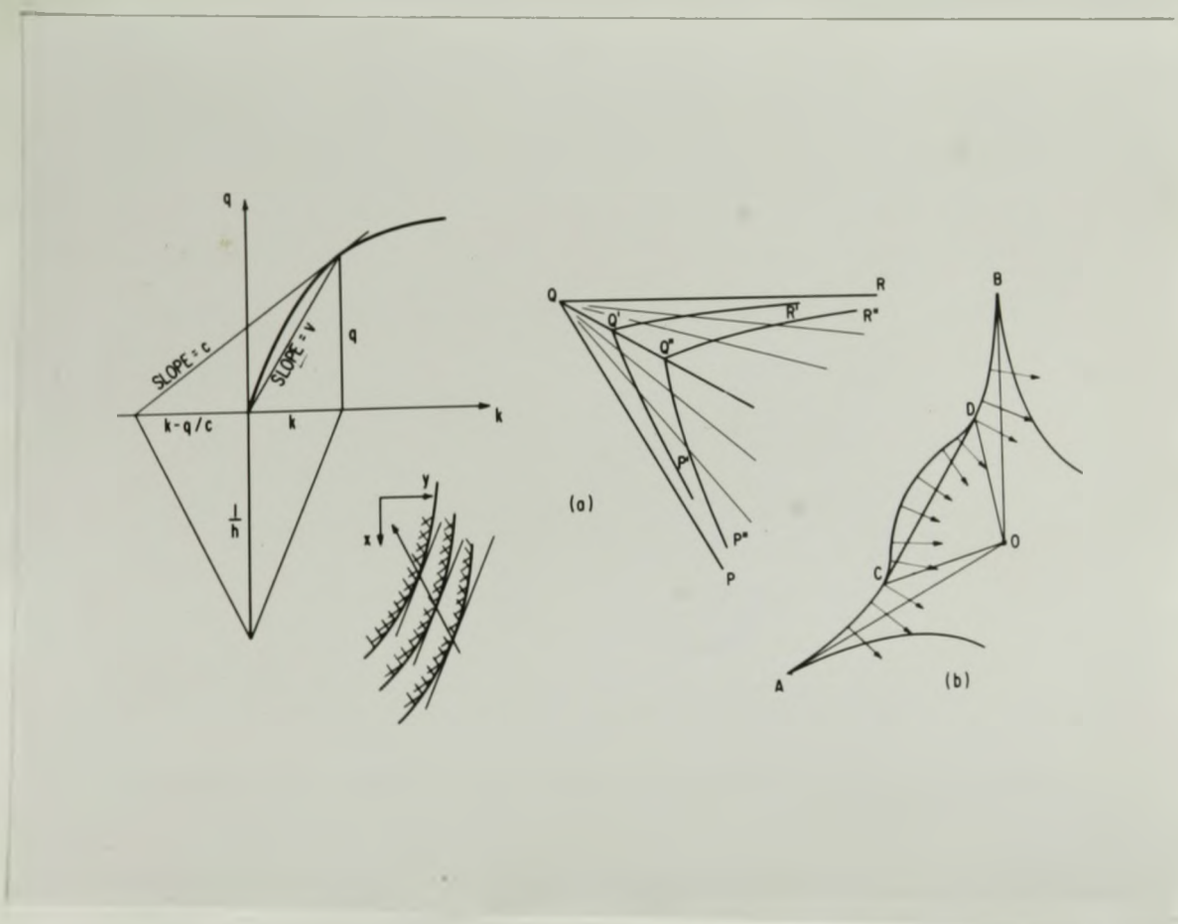

FIGURE 2: Relationship between step flux (q) and step density (k) and geometrical construction for the orientation trajectories from this.

(a) Dissolution at a crystal edge, corresponding to the polar diagram of reciprocal dissolution rate shown in (b).

(Adapted from "Growth and Perfection of Crystals", edited by R. H. Doremus, B. W. Roberts and D. Turnbull, John Wiley and Sons, New York, 1958, p. 413.)

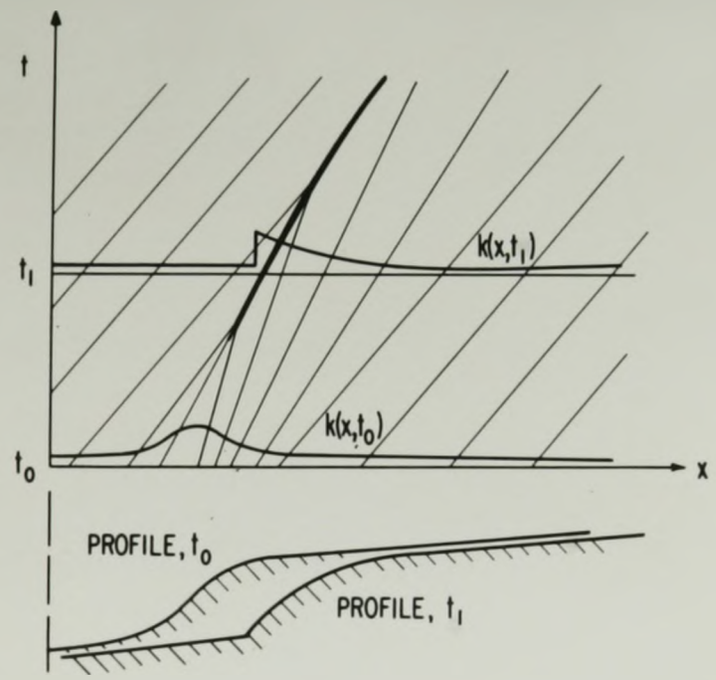

Fig. 3 Progressive displacement and change of shape of a step bunch.

(Adapted from "Growth and Perfection of Crystals", edited by R. H. Doremus, B. W. Roberts and D. Turnbull, John Wiley and Sons, New York, 1958, p. 415.)

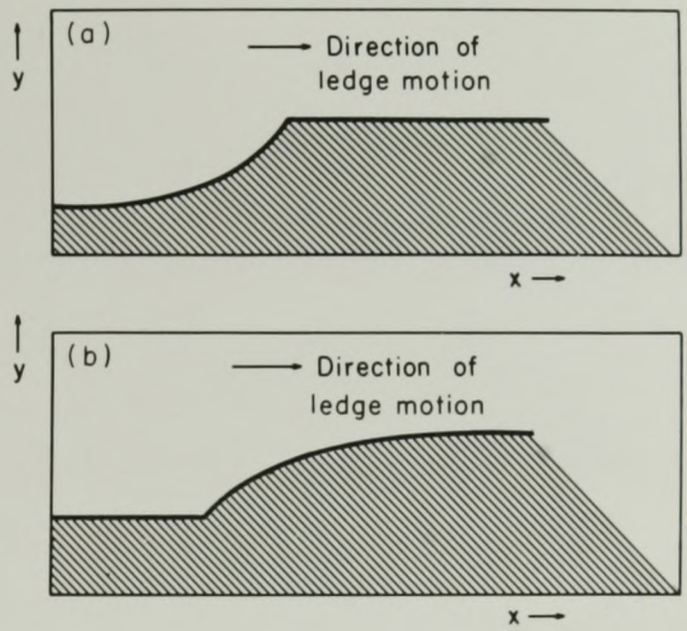

Fig. 8. Surface profiles arising from step bunches with (a) *positive* $d^2q/d\kappa^2$, *and* (b) *negative* $d^2q/d\kappa^2$

(Adapted from "Metal Surfaces", American Society for Metals, Metals Park, Ohio, 1963, p. 209.)

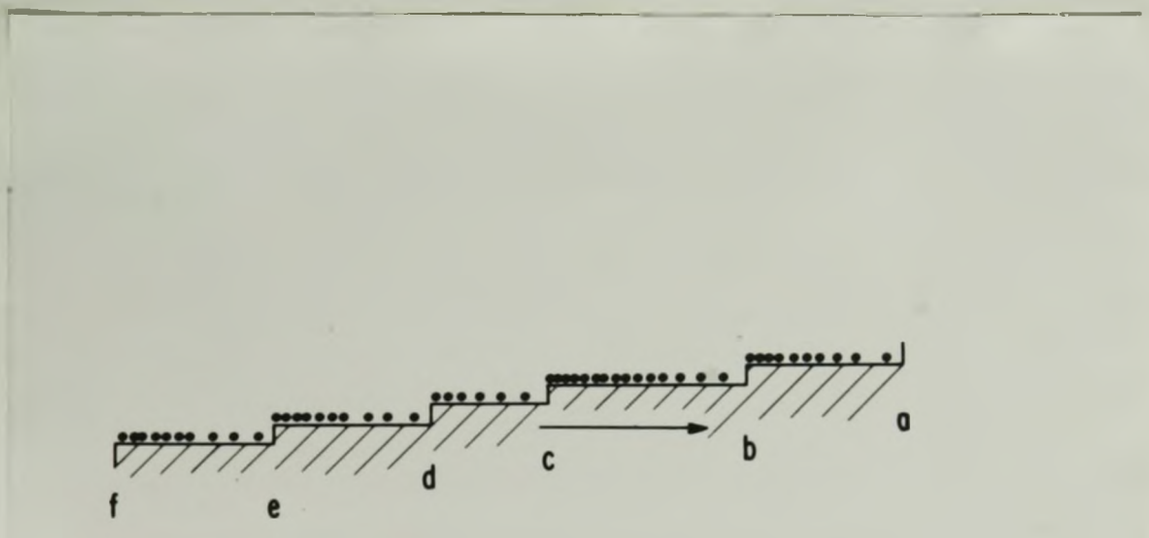

FIGURE 5: Effect of time-dependent adsorption on a perturbation from regularity of a step sequence.

(Adapted from "Growth and Perfection of Crystals", edited by R. H. Doremus, B. W. Roberts and D. Turnbull, John Wiley and Sons, New York, 1958, p. 417.)

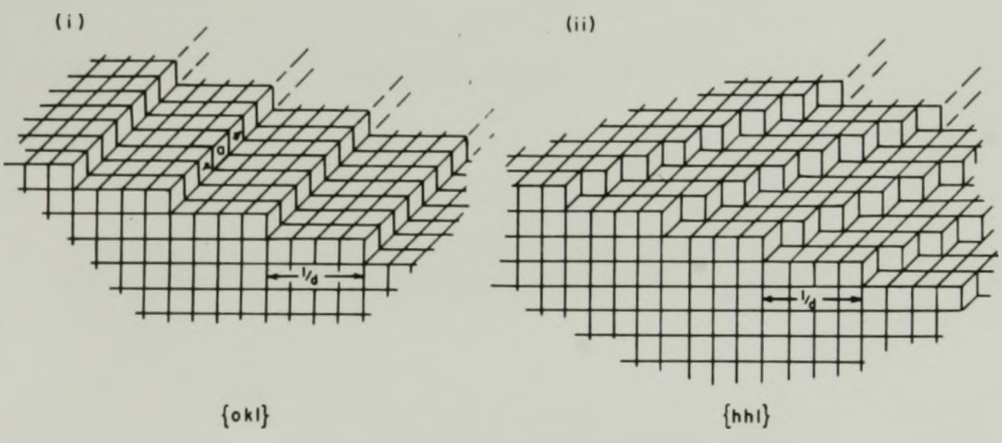

FIGURE 6: Building model of (i) a ledge-surface {okl} and (ii) a kink surface {hhl} on an alkali halide crystal, using Kossel's concept.

(Adapted from M. B. Ives, J. Phys. Chem. Solids 24, 275 (1963).)

(a)

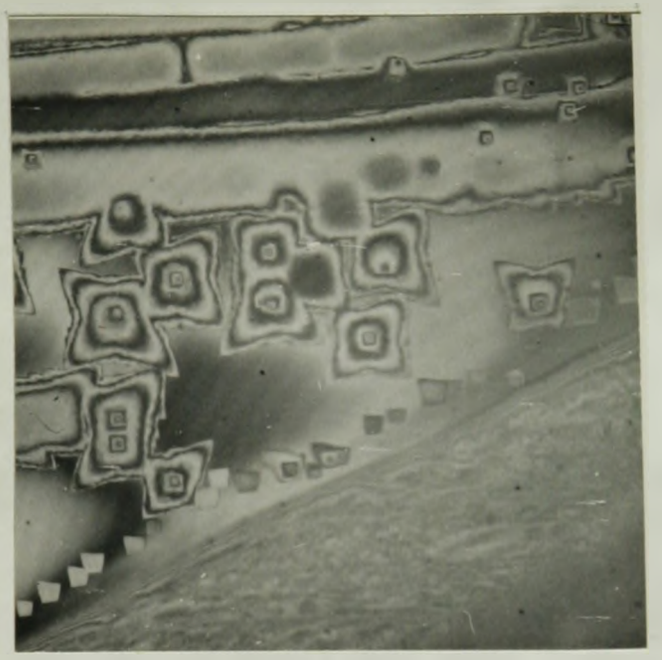

(b)

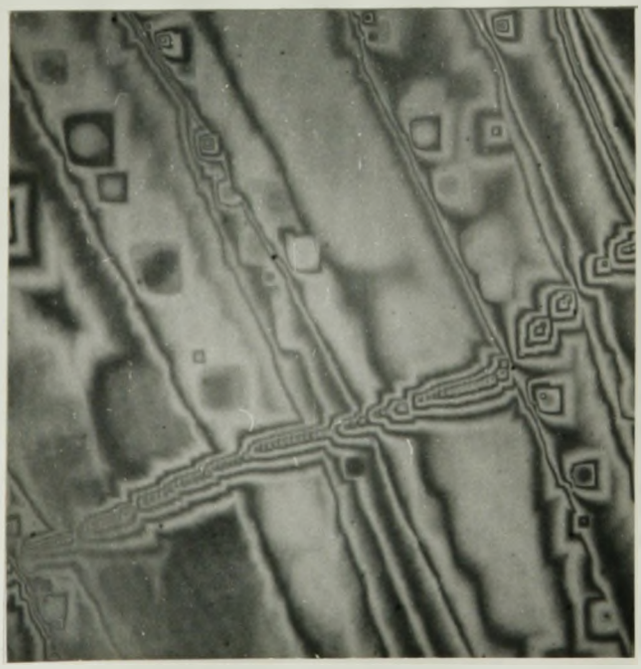

FIGURE 7: Interference micrographs of etch pits on lithium fluoride etched for 2 minutes in solutions of ferric chloride containing (a) 0.3 p.p.m. Fe, (b) 1.5 p.p.m. Fe.

(c)

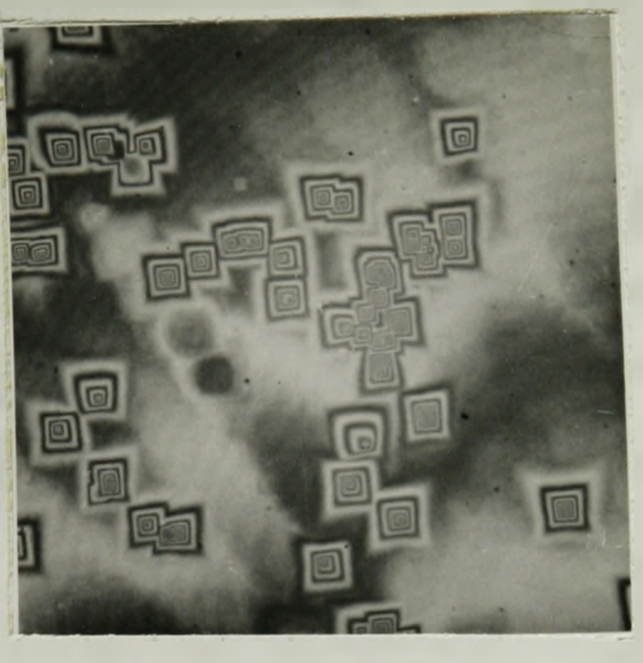

(d)

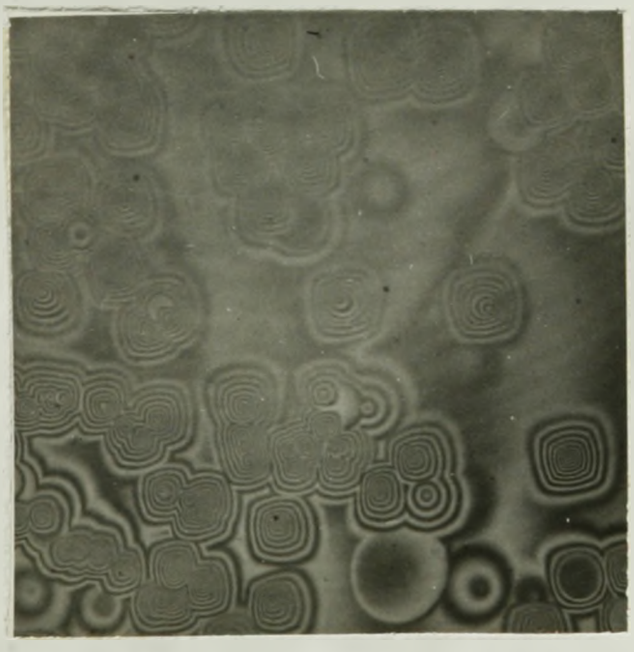

FIGURE 7: Interference micrographs of etch pits on lithium fluoride etched for 2 minutes in solutions of ferric chloride containing (c) 3 p.p.m. Fe, (d) 15 p.p.m. Fe.

(e)

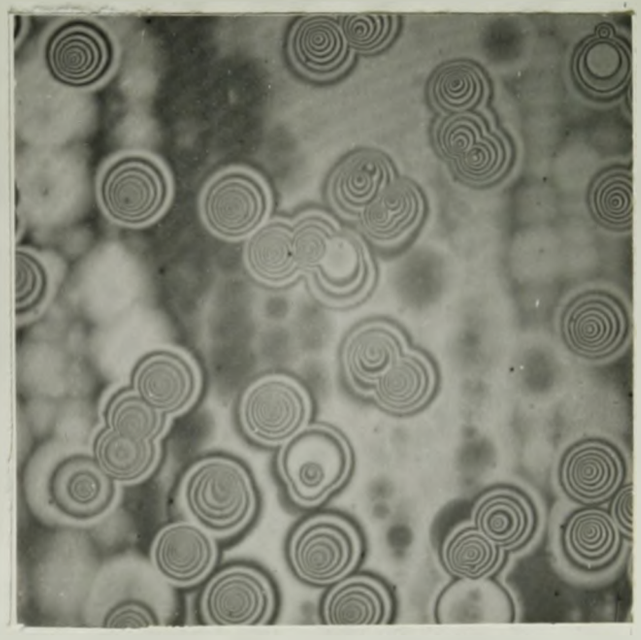

FIGURE 7: Interference micrographs of etch pits on lithium fluoride etched for 2 minutes in solutions of ferric chloride containing (e) 150 p.p.m. Fe.

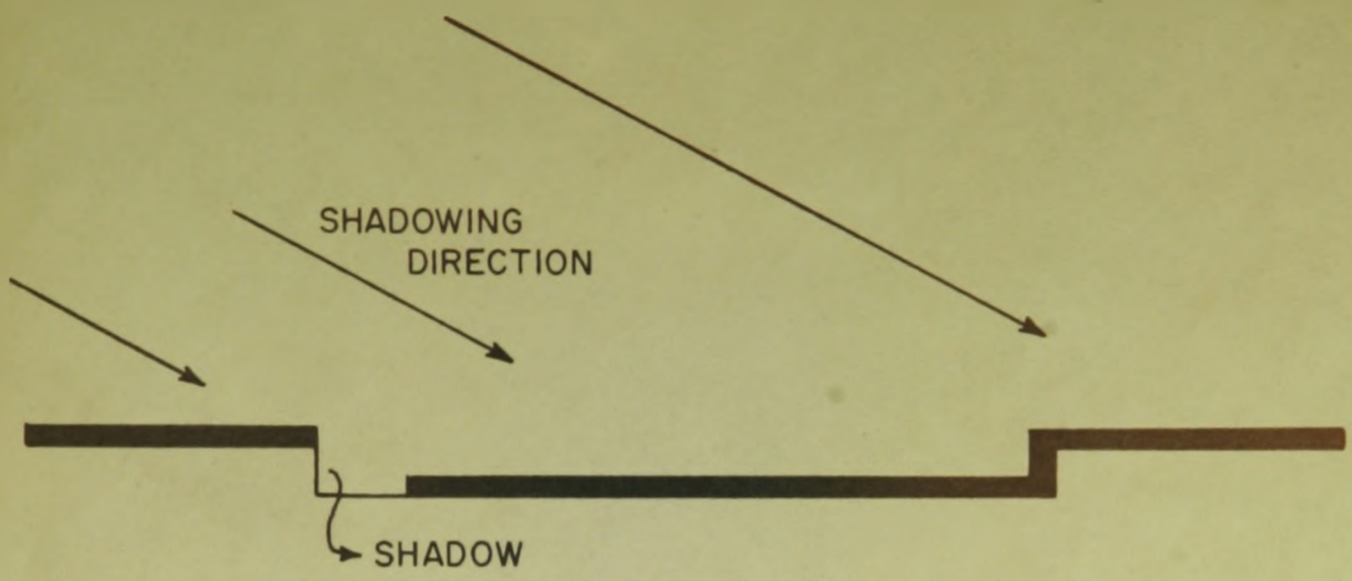

FIGURE 8: A simple diagram of an etch pit with only one step showing the shadowed region.

FIGURE 9: Experimental set up for the evaporation of gold and platinum-carbon pellets

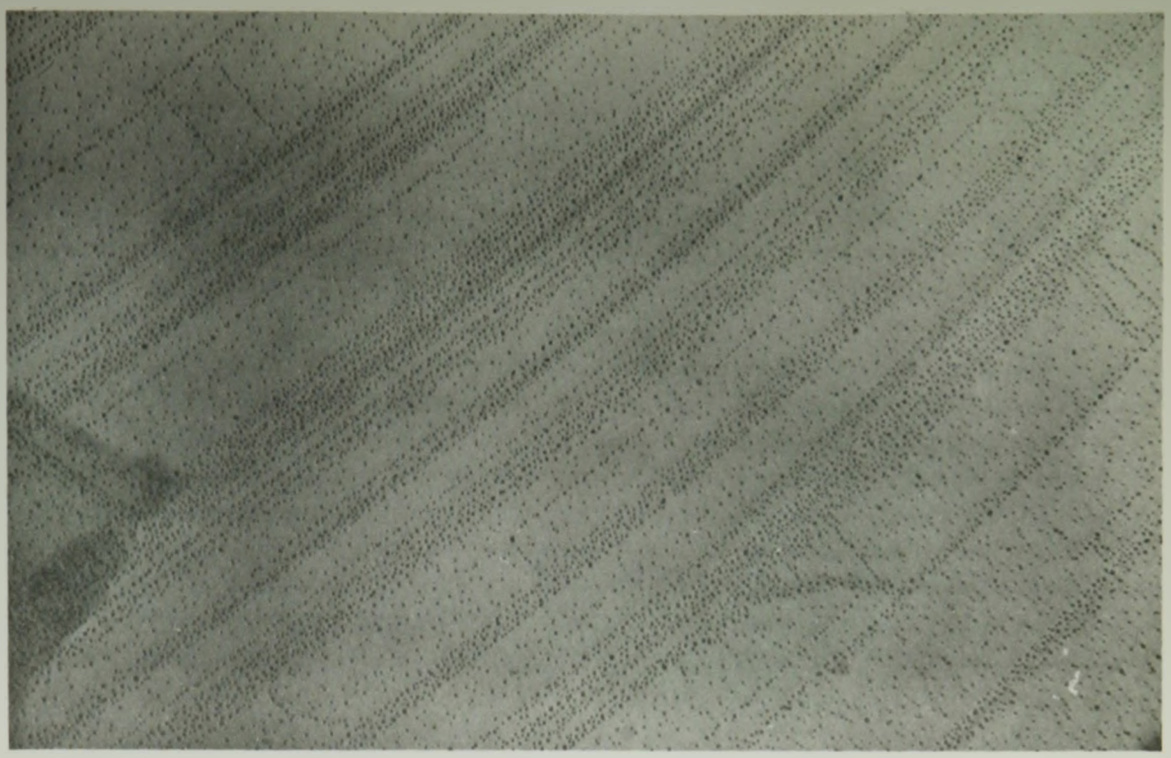

FIGURE 10: Nucleation of gold on cleavage surface of lithium fluoride at 200°C. (110,000 X)

FIGURE 11: Nucleation of gold on cleavage surface of lithium fluoride at 300°C. (100,000 X)

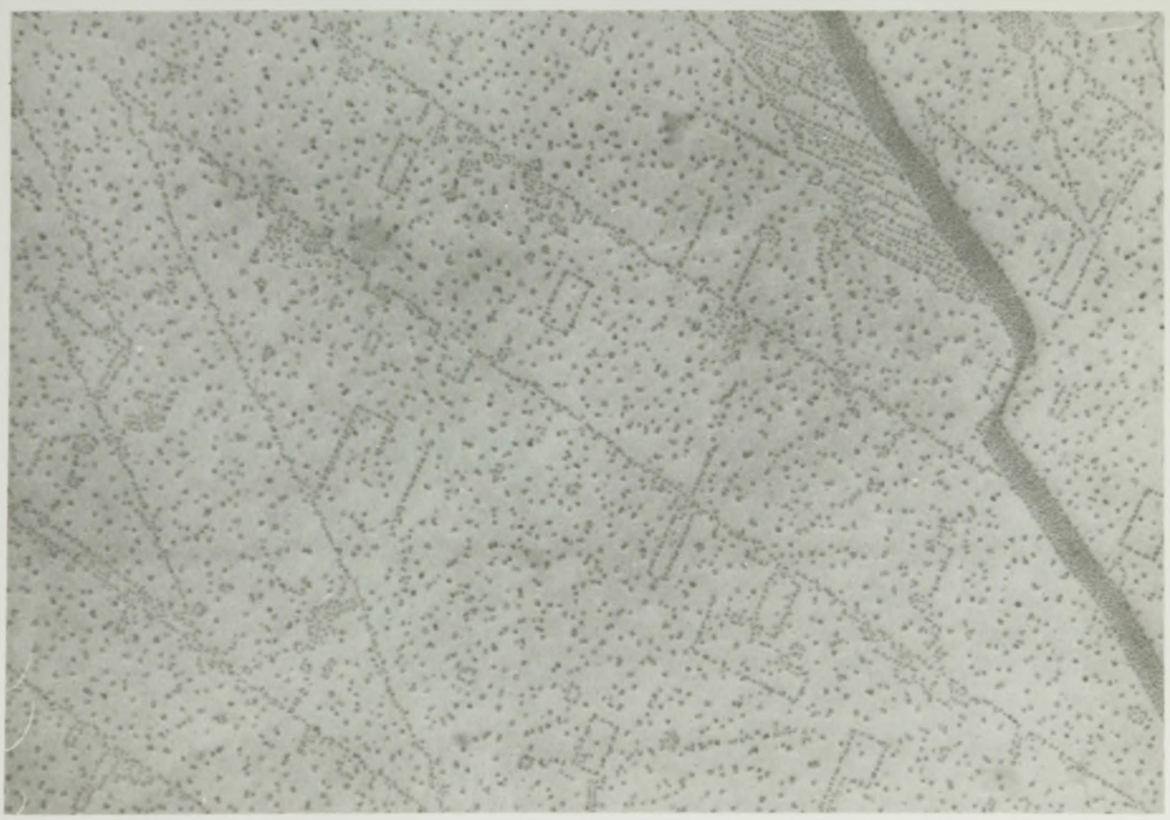

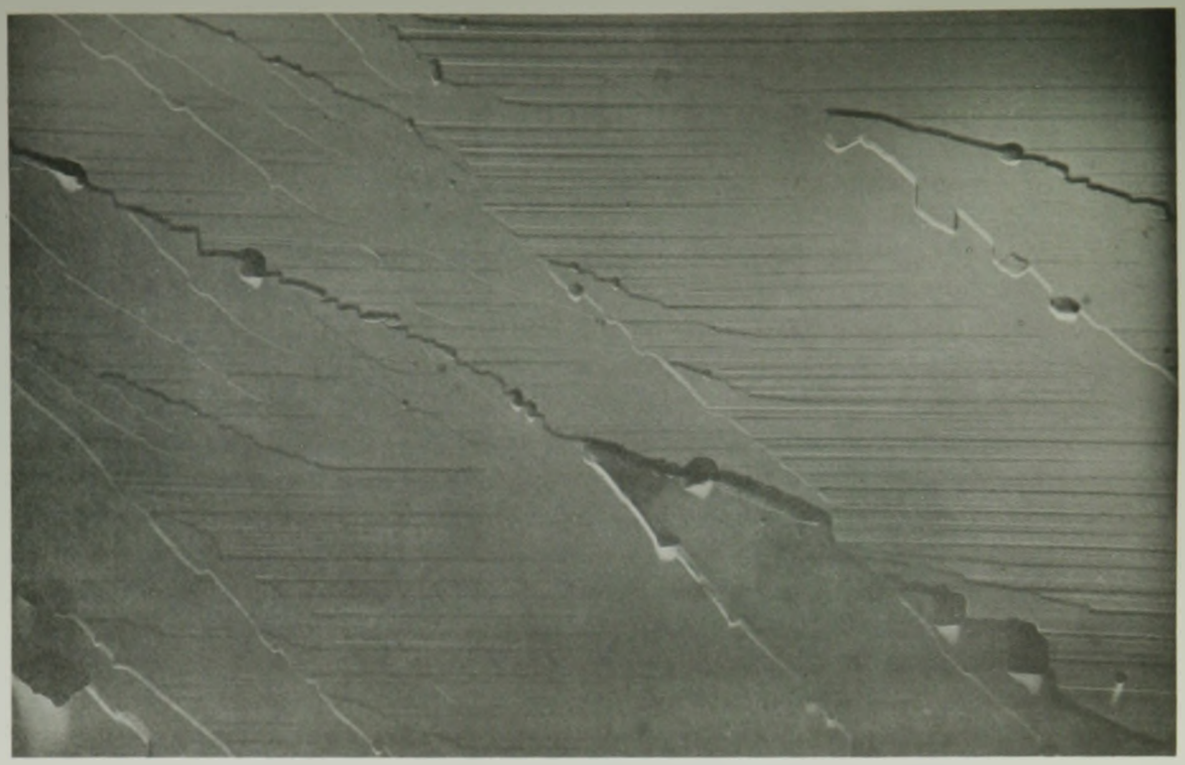

FIGURE 12: Platinum-carbon replica of cleaved lithium fluoride surface (16,000 X)

FIGURE 13: Platinum-carbon replica of lithium fluoride surface etched with distilled water (16,000 X)

Etching time 30 seconds

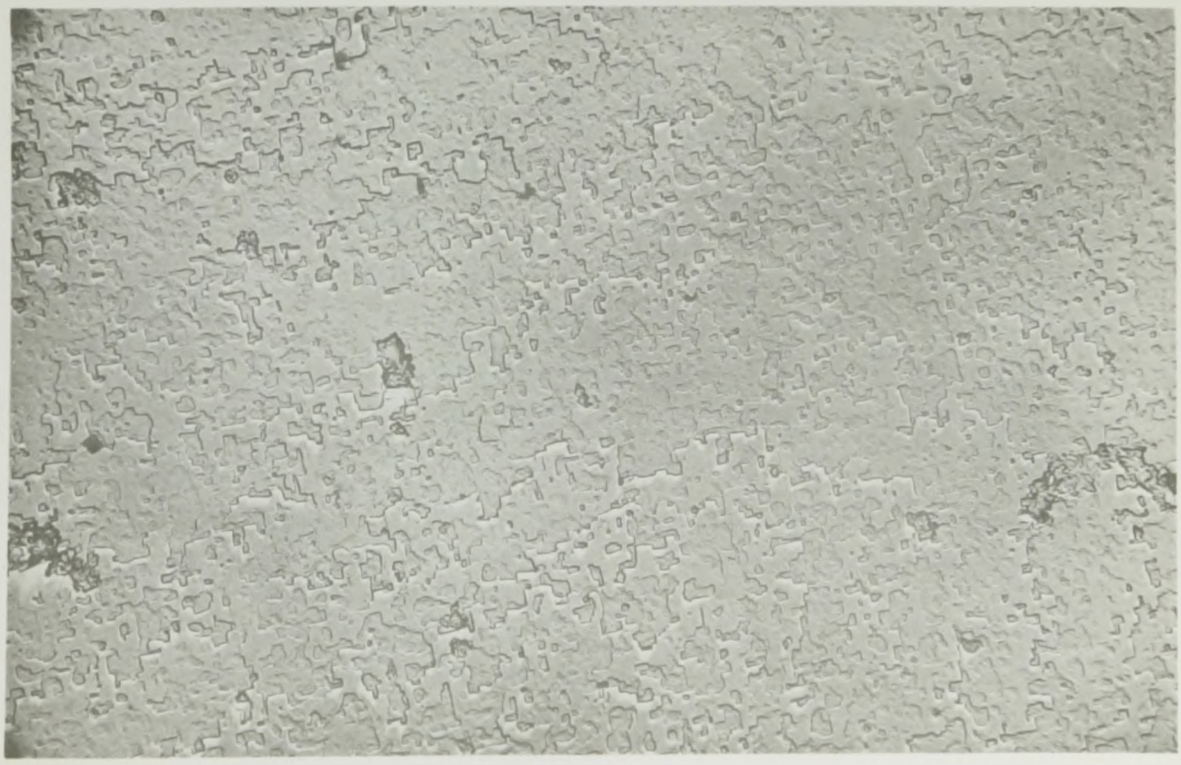

FIGURE 14

Platinum-carbon replicas of surfaces of lithium fluoride polished with 1.5% ammonium hydroxide (20,000 X)

FIGURE 15

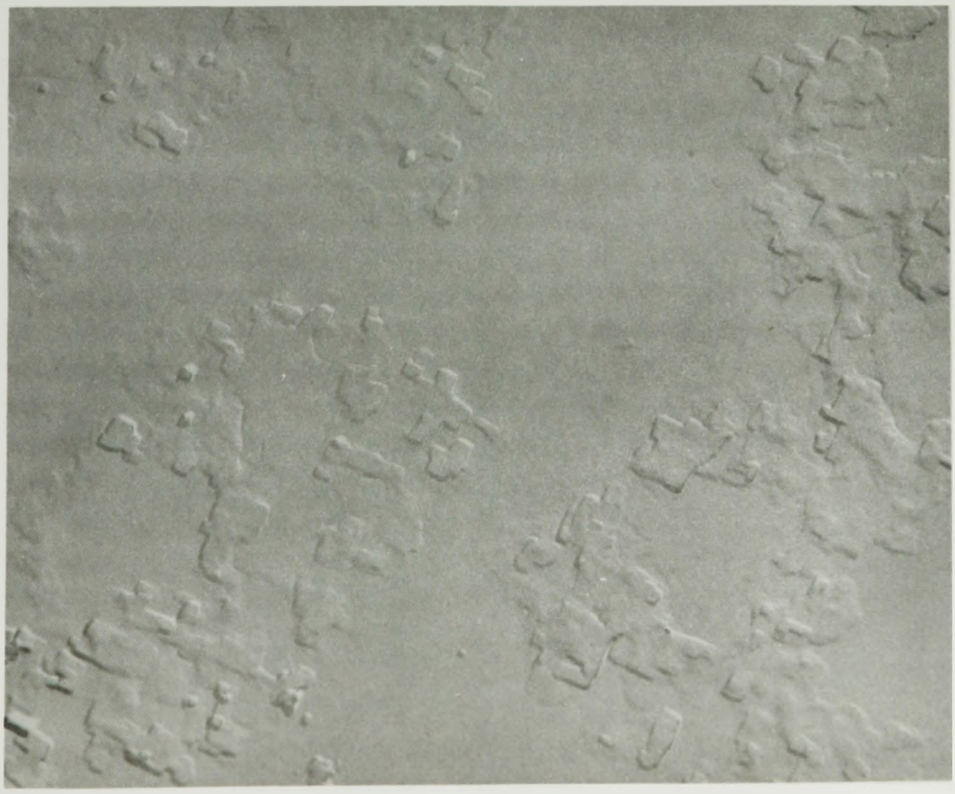

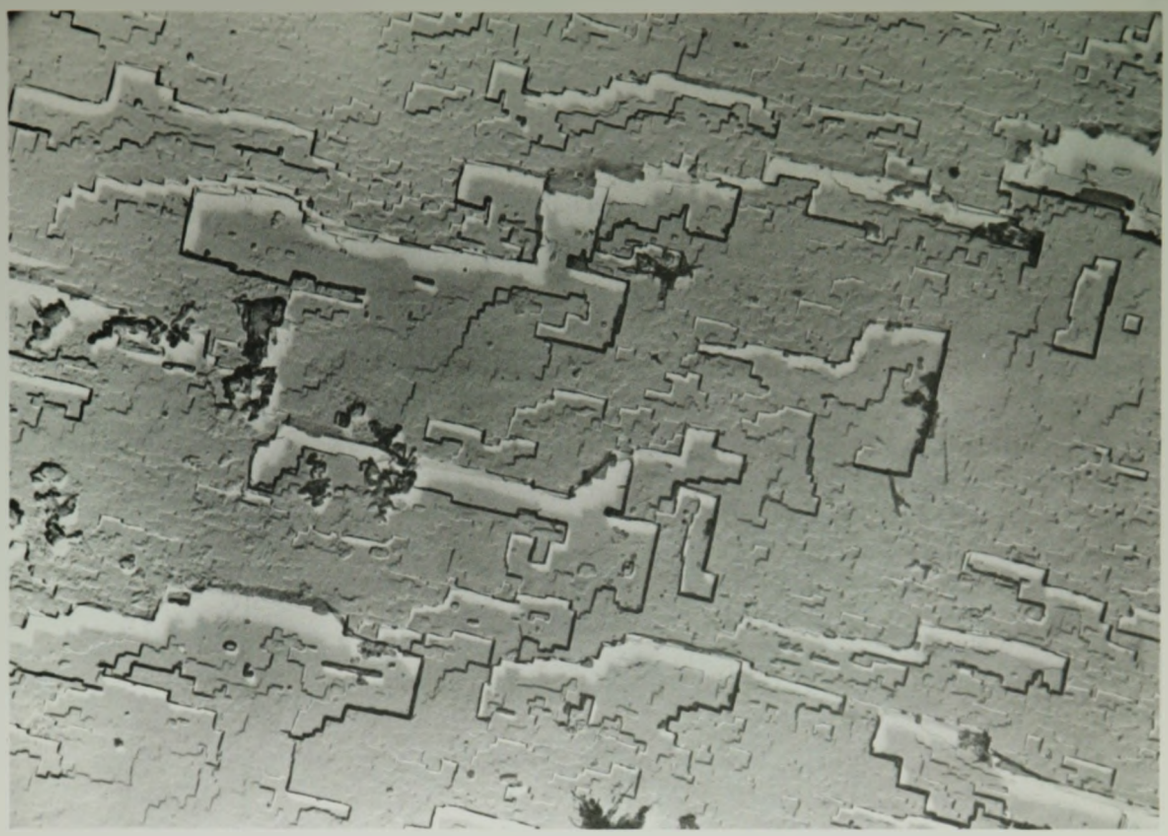

FIGURE 16: Instantaneous etch (16,000 X)

Inhibitor concentration 0.3 p.p.m. Fe

FIGURE 17: 30 second etch (16,000 X)

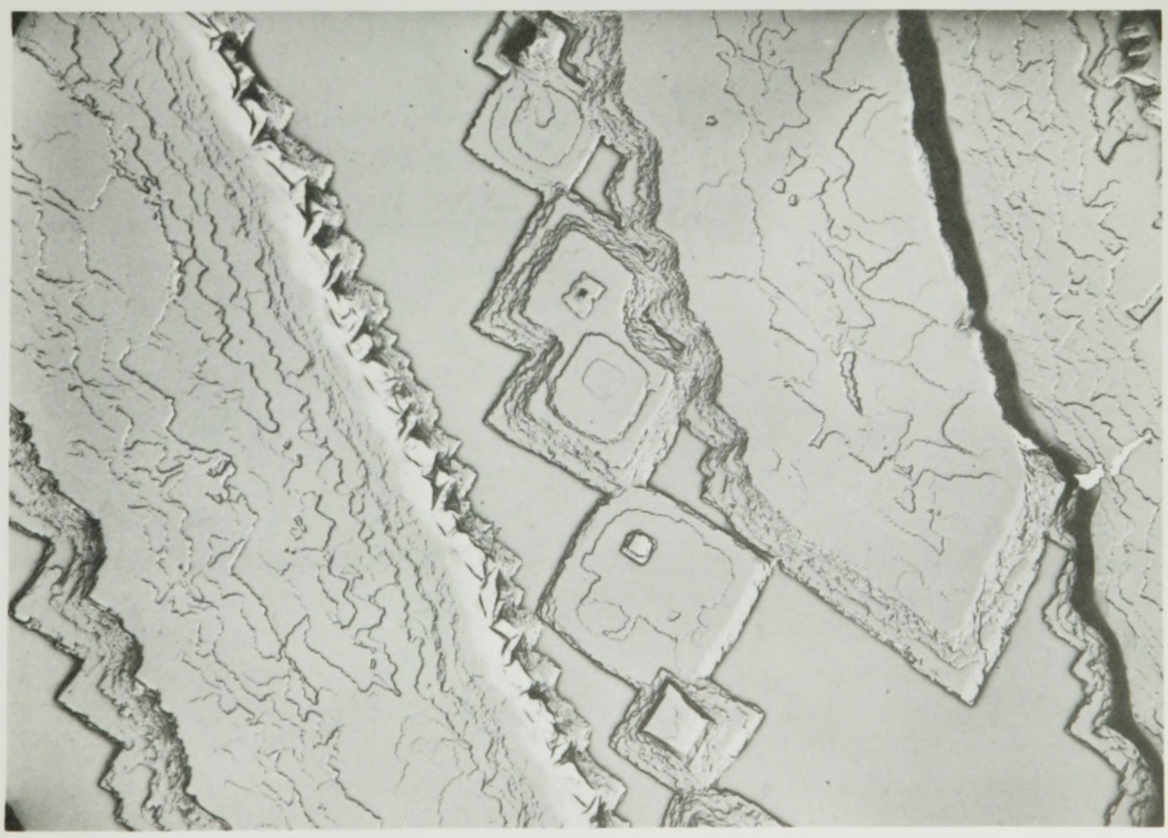

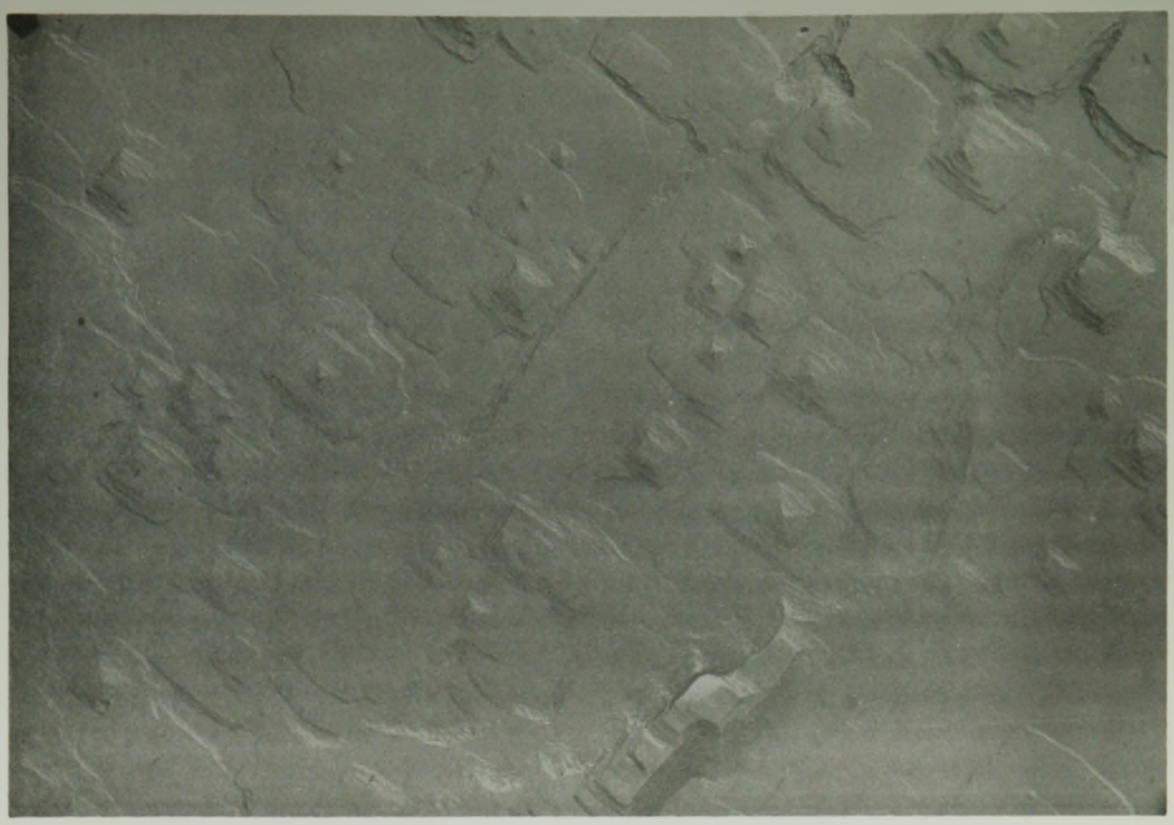

FIGURE 18: Instantaneous etch (16,000 X)

Inhibitor concentration 1.5 p.p.m. Fe

FIGURE 19: 30 second etch (16,000 X)

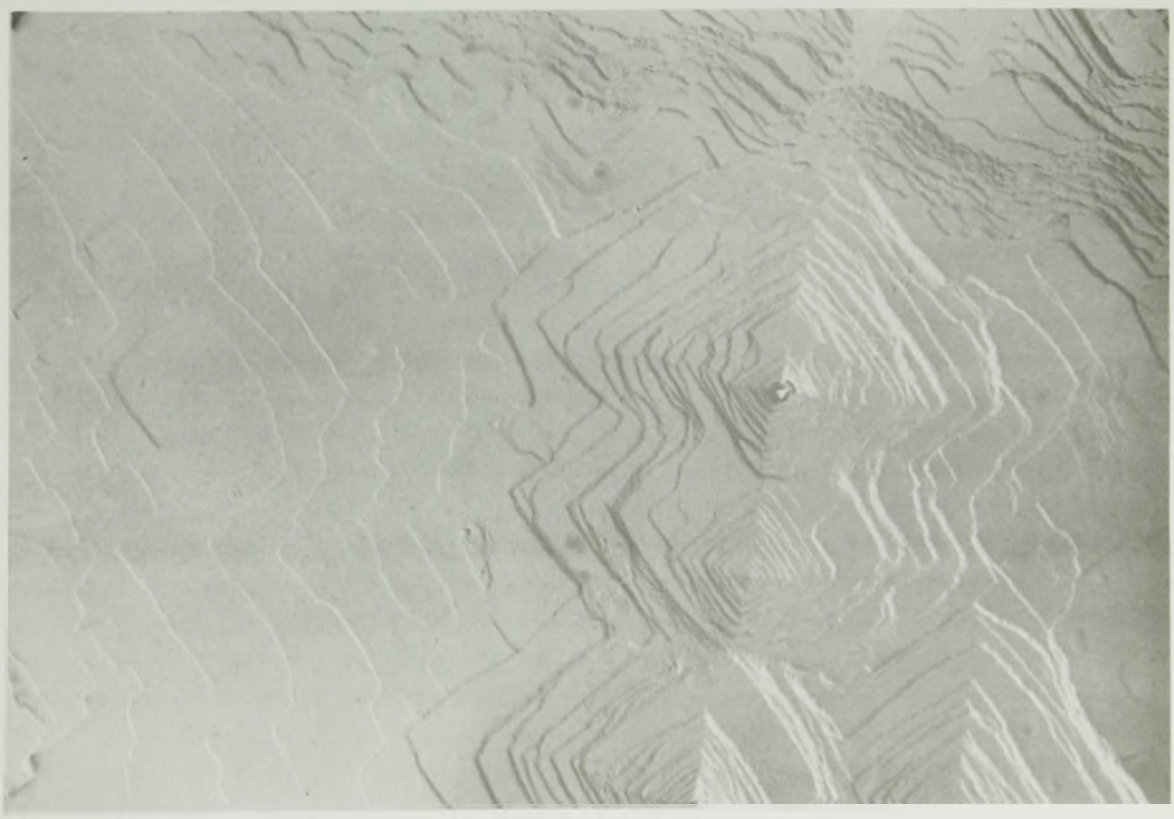

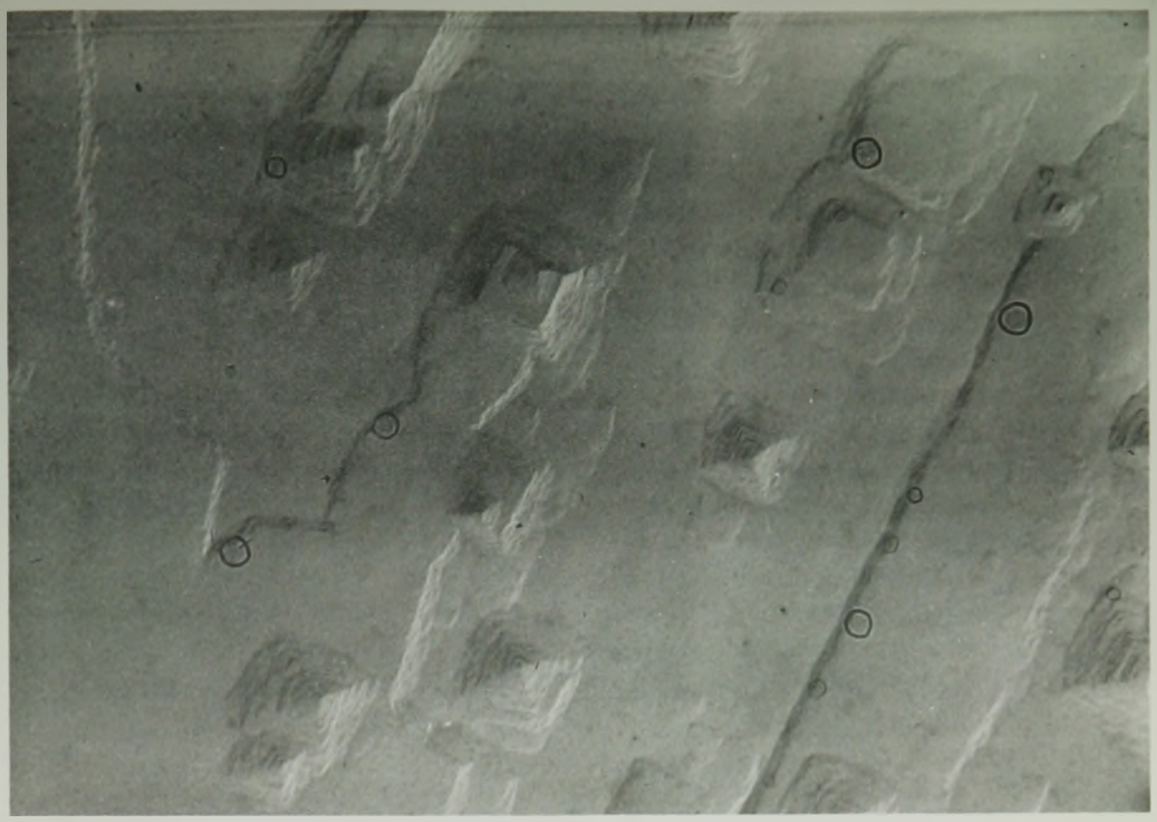

FIGURE 20: Instantaneous etch (16,000 X)

Inhibitor concentration 6 p.p.m. Fe

FIGURE 21: 30 second etch (16,000 X)

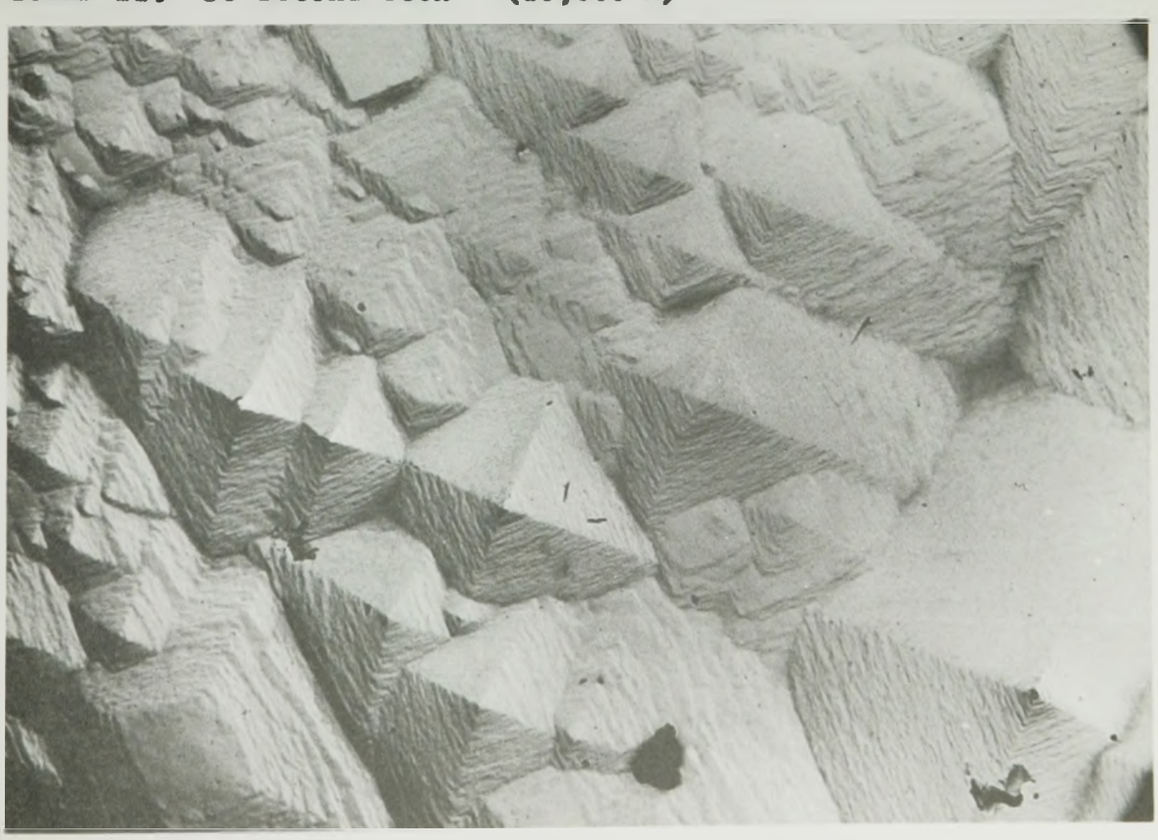

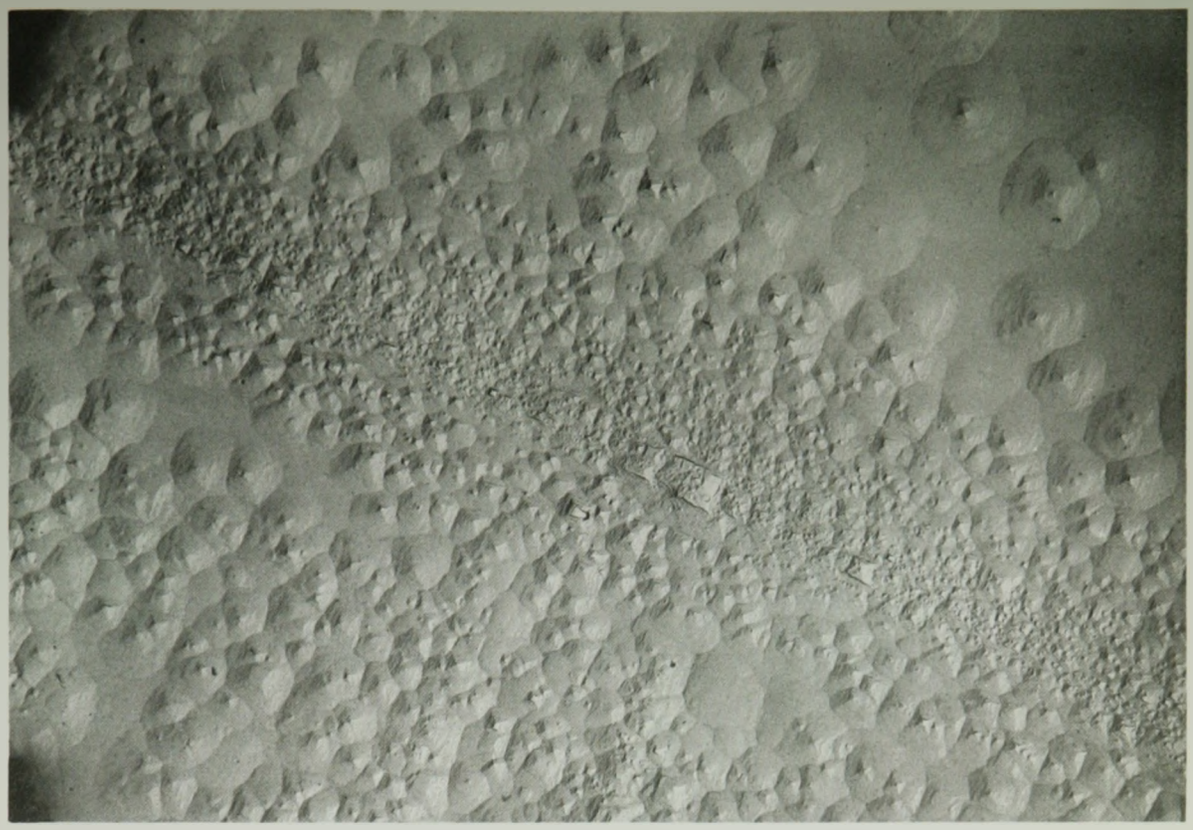

FIGURE 22: Instantaneous etch (16,000 X)

Inhibitor concentration 15 p.p.m. Fe

FIGURE 23: 30 second etch (16,000 X)

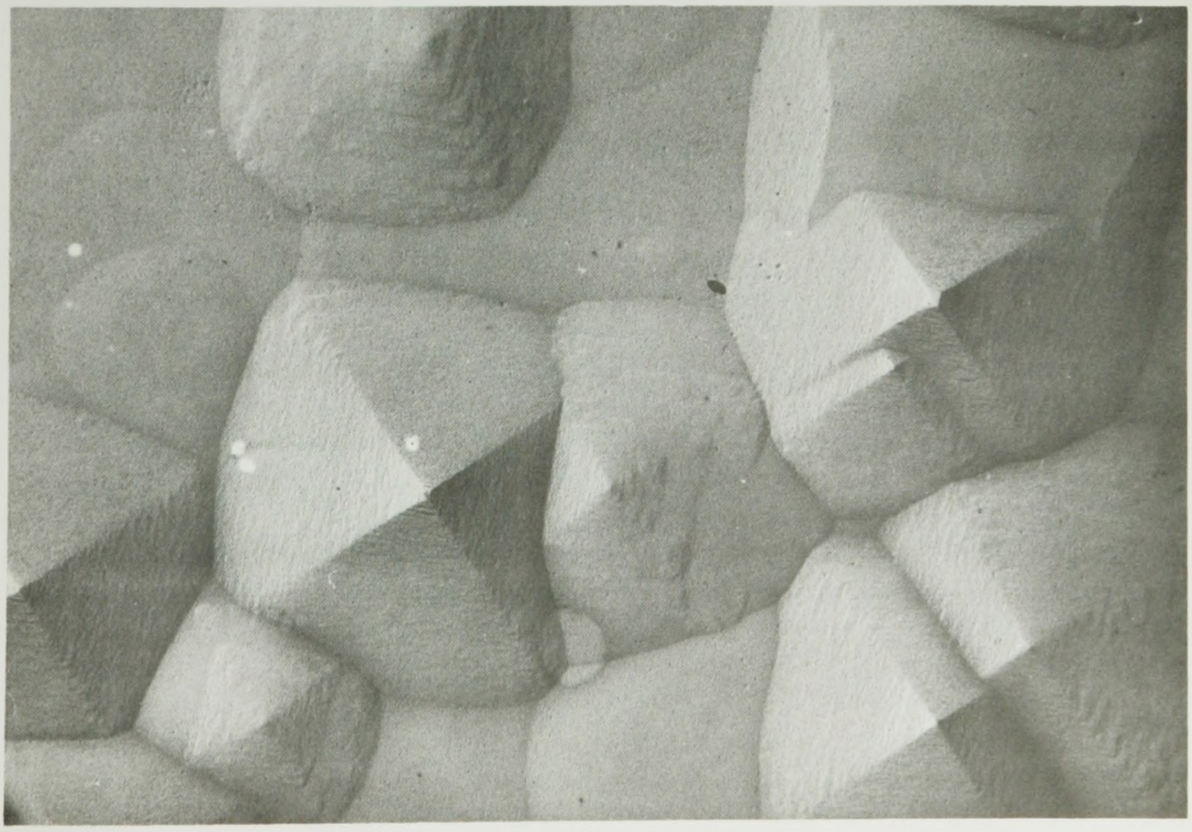

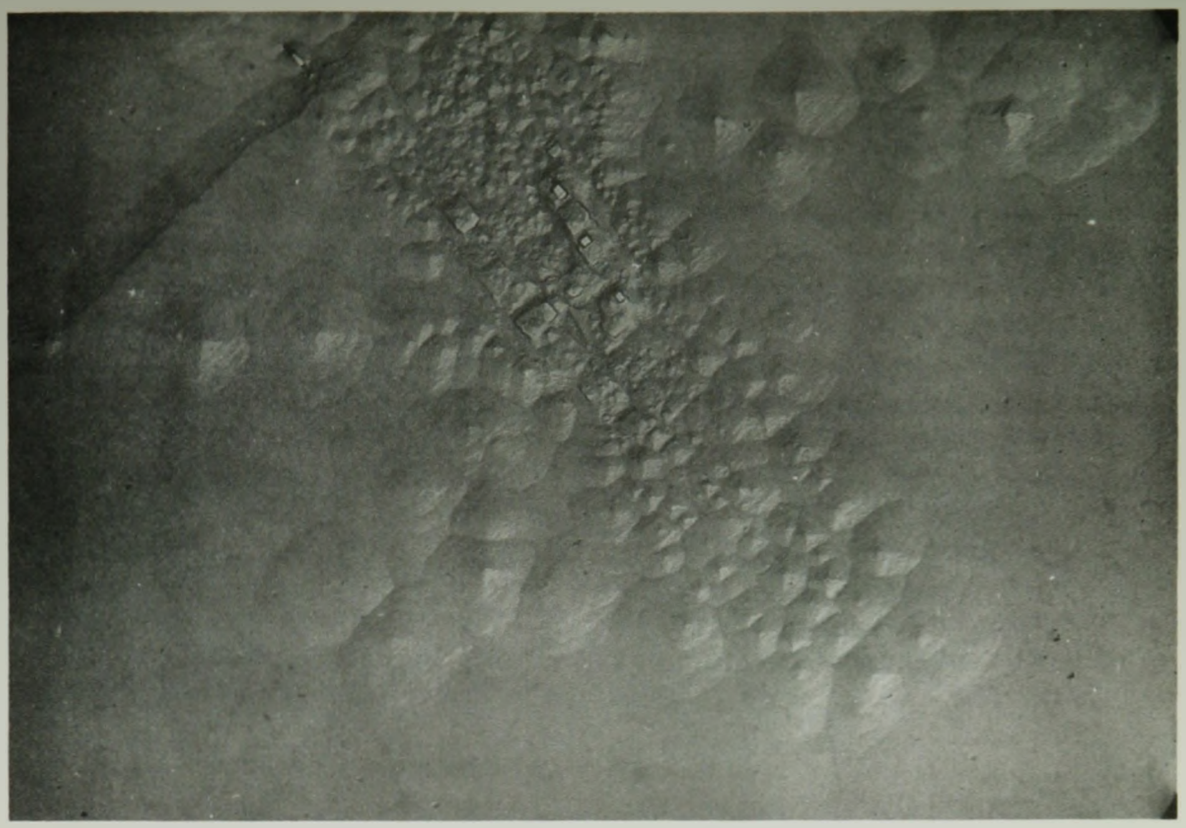

FIGURE 24: Instantaneous etch (16,000 X)

Inhibitor concentration 30 p.p.m. Fe

FIGURE 25: 30 second etch (16,000 X)

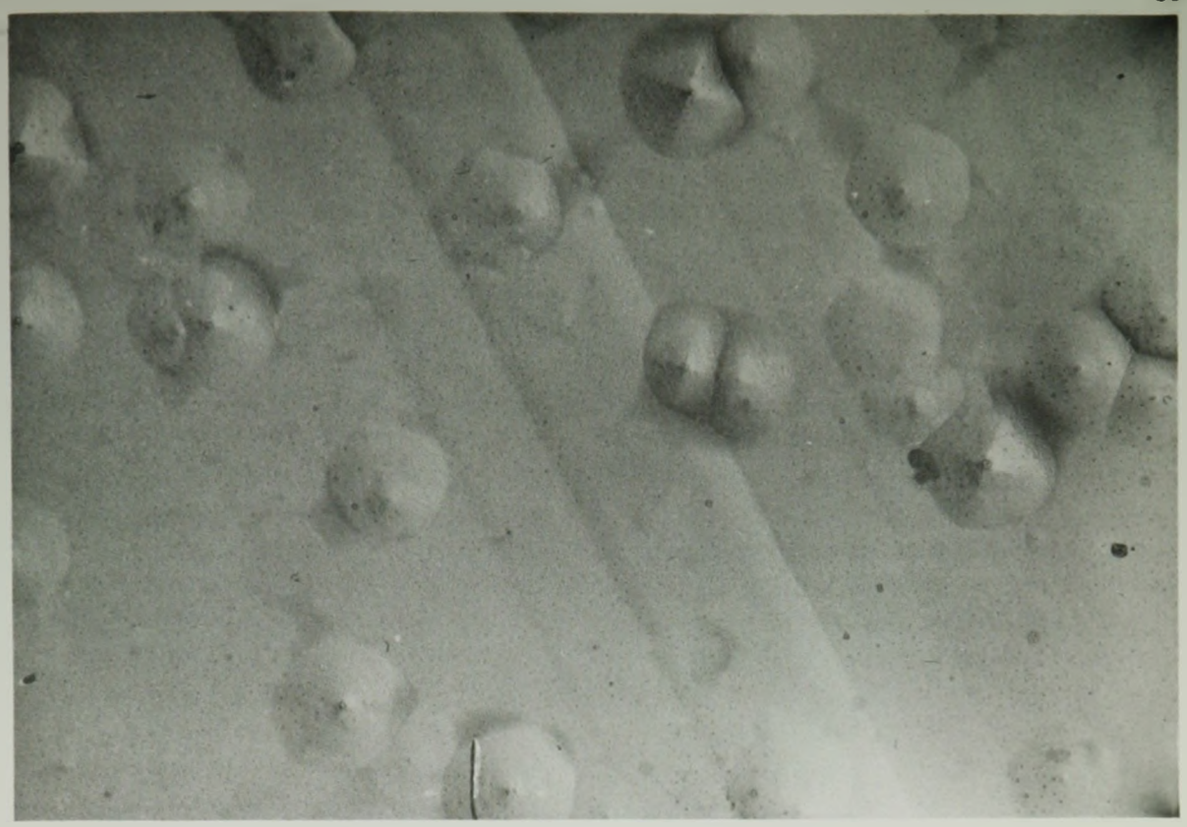

FIGURE 26: Instantaneous etch (16,000 X)

Inhibitor concentration 60 p.p.m. Fe

FIGURE 27: 30 second etch (16.000 X)

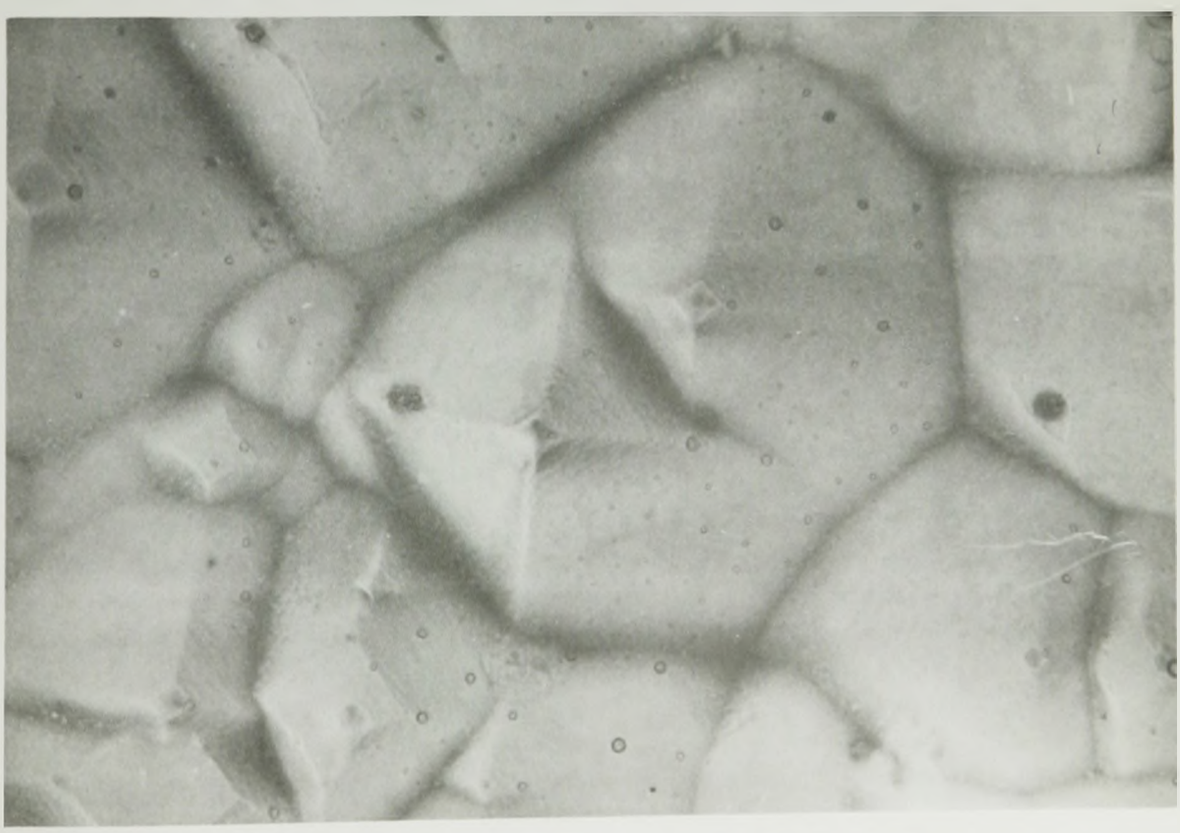

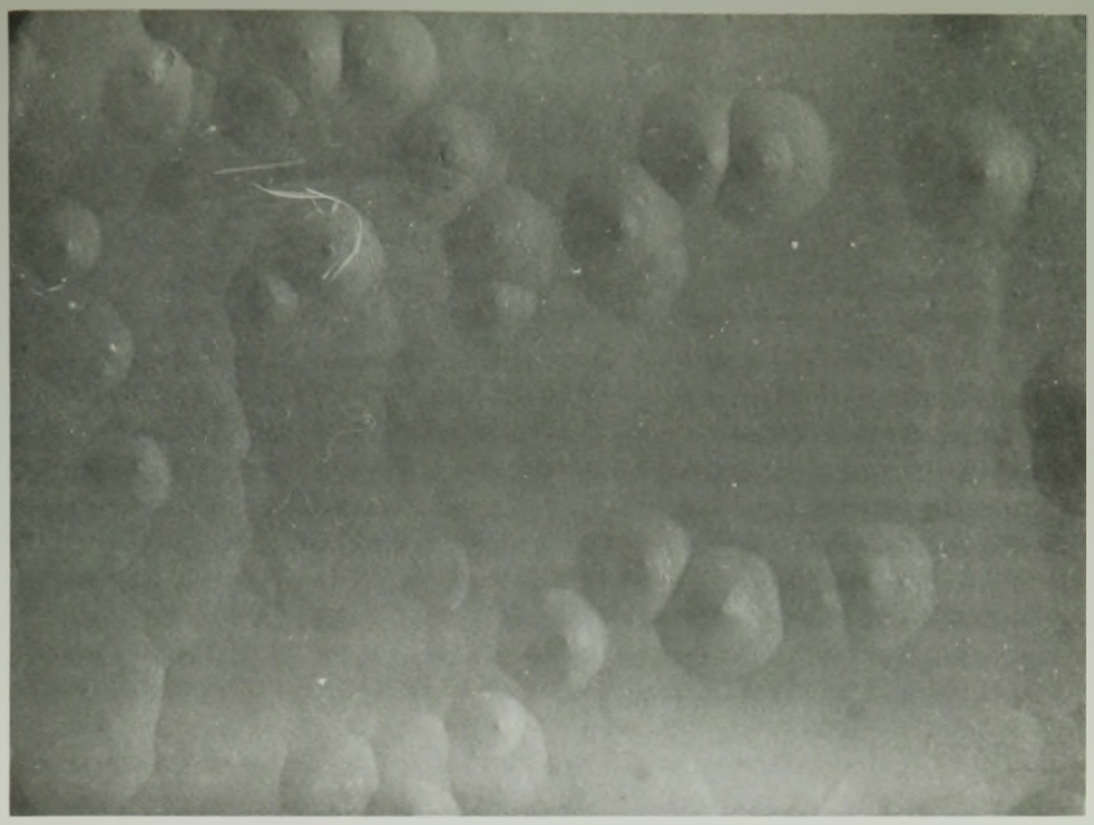

FIGURE 28: Instantaneous etch (16,000 X)

Inhibitor concentration 150 p.p.m. Fe

FIGURE 29: 30 second etch (16,000 X)

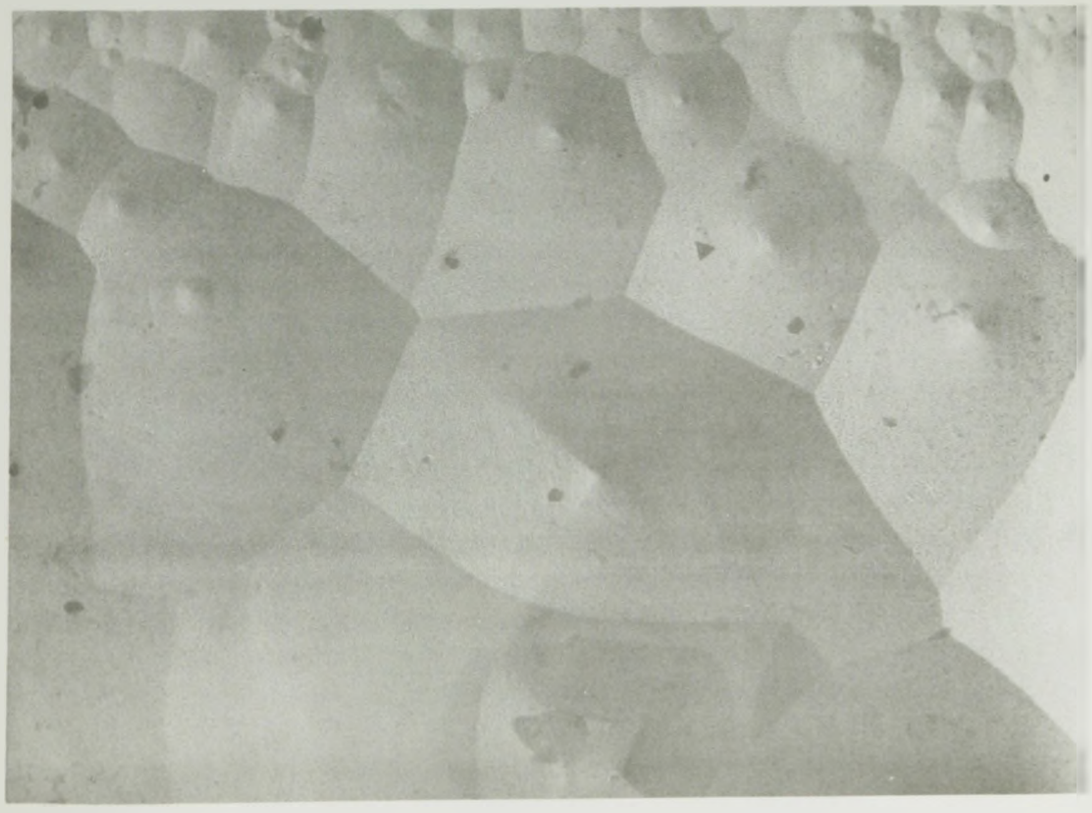

FIGURE 30

Inhibitor concentration 1.5 p.p.m. Fe
Time of etching 2 minutes (16,000 X)

FIGURE 31

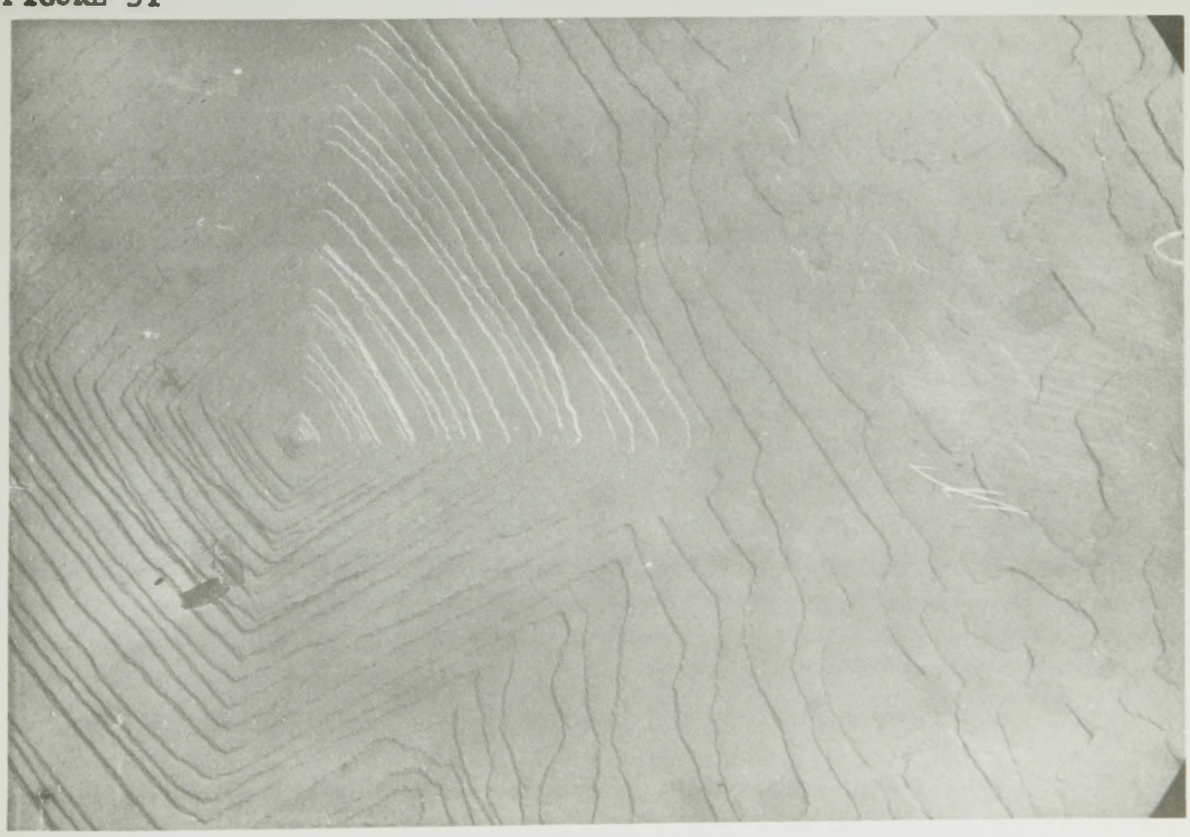

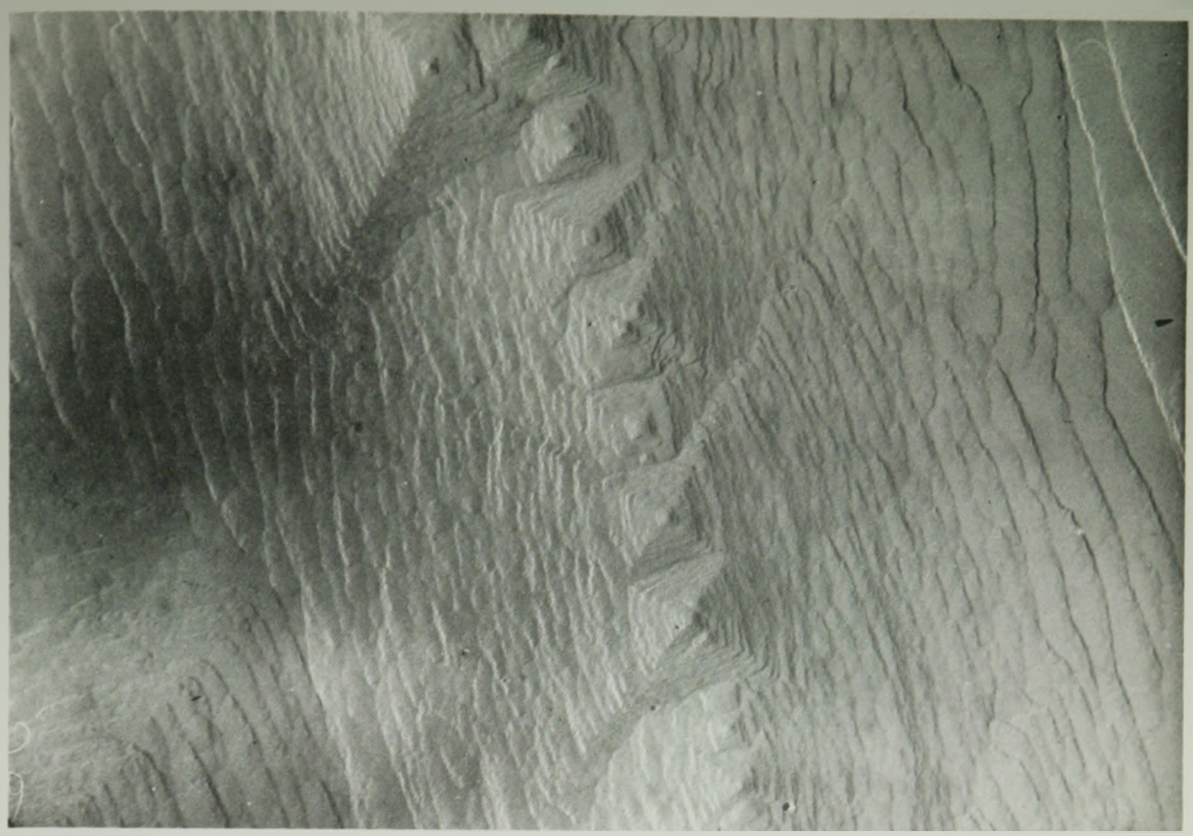

FIGURE 32

Inhibitor concentration 3 p.p.m. Fe
Time of etching 30 seconds (16,000 X)

FIGURE 33

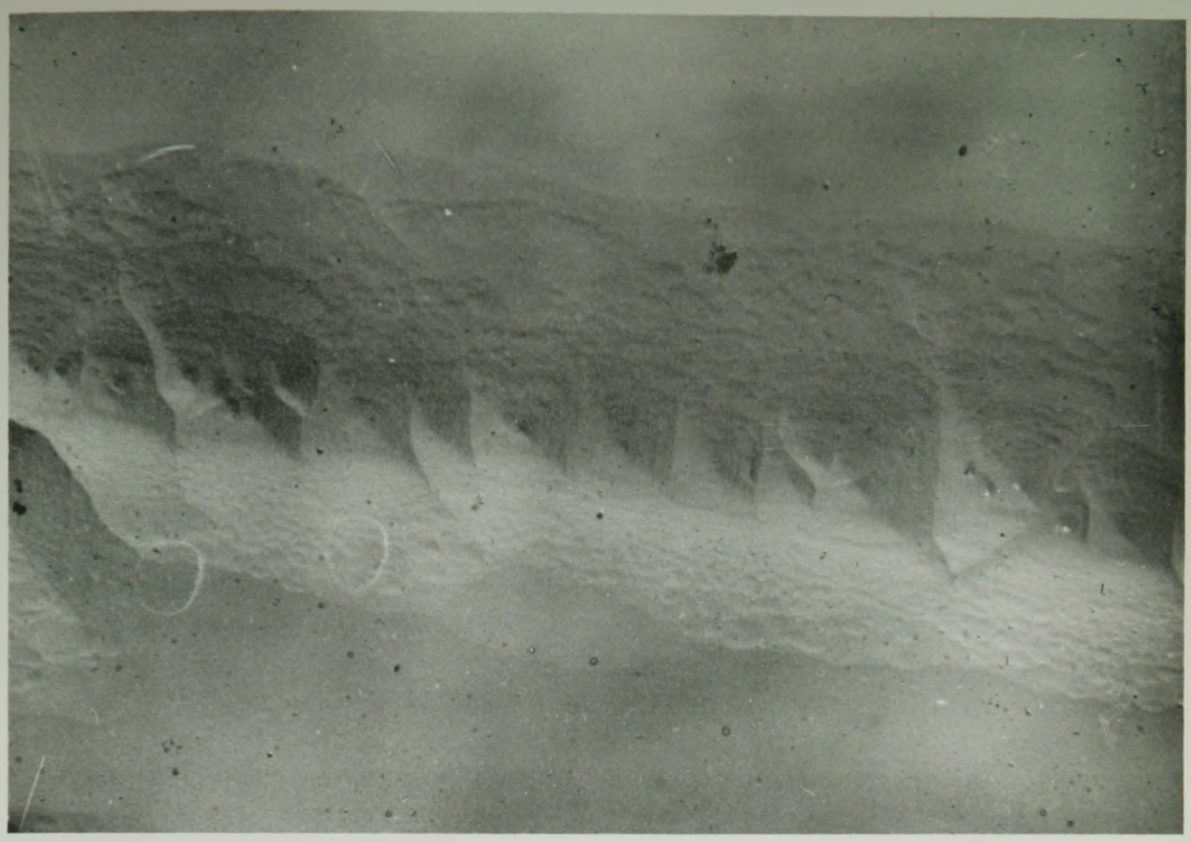

FIGURE 34: Time of etching 30 seconds (16,000 X)

Inhibitor concentration 9 p.p.m. Fe

FIGURE 35: Time of etching 2 minutes (16,000 X)

FIGURE 36: Inhibitor concentration 9 p.p.m. Fe.
Time of etching 5 seconds (16,000 X)

FIGURE 37: Inhibitor concentration 0.3 p.p.m. Fe.
Time of etching 2 minutes (16,000 X)

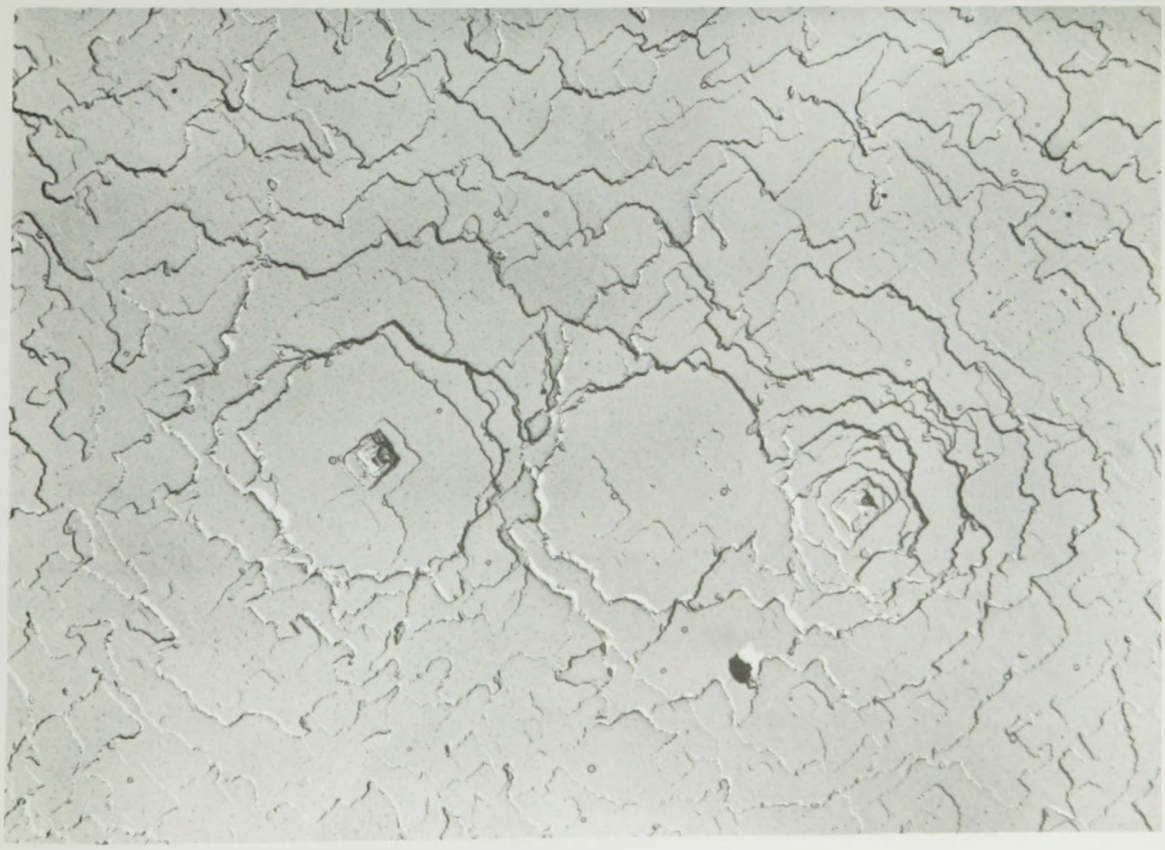

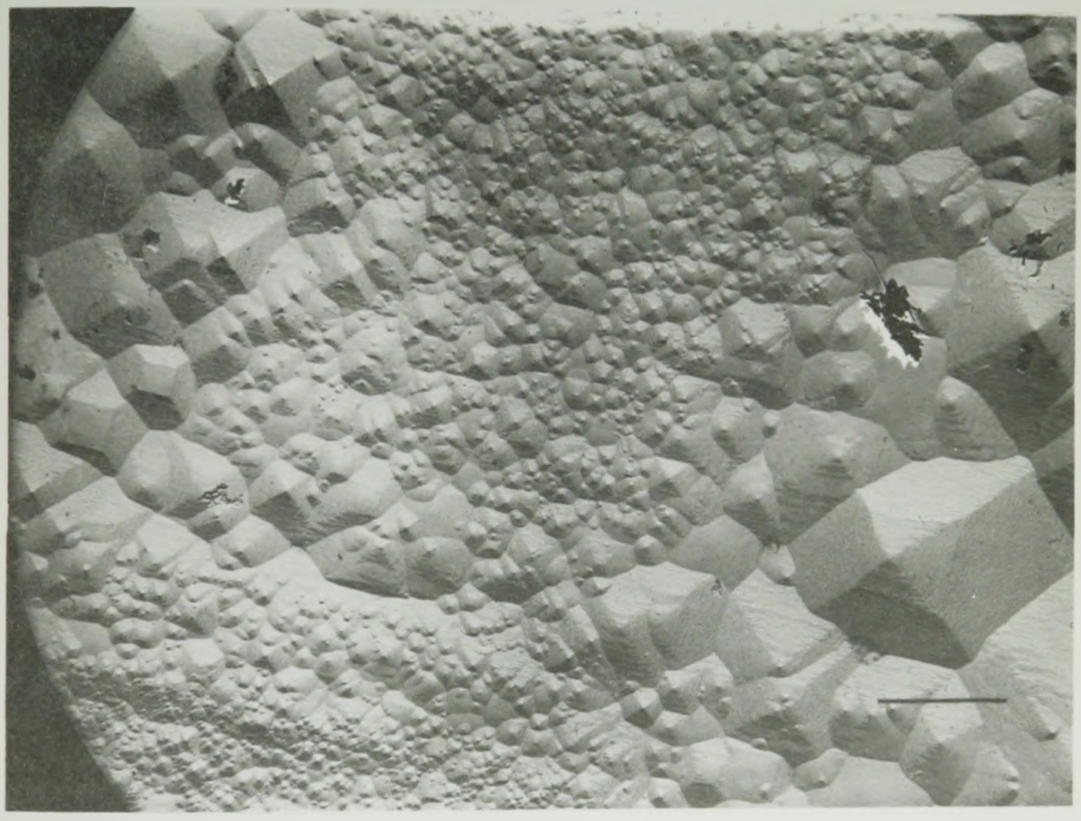

FIGURE 38: Inhibitor concentration 9 p.p.m. Fe.
Time of etching 2 minutes

FIGURE 39

Inhibitor concentration 6 p.p.m. Fe
Time of etching 30 seconds (16,000 X)

FIGURE 40

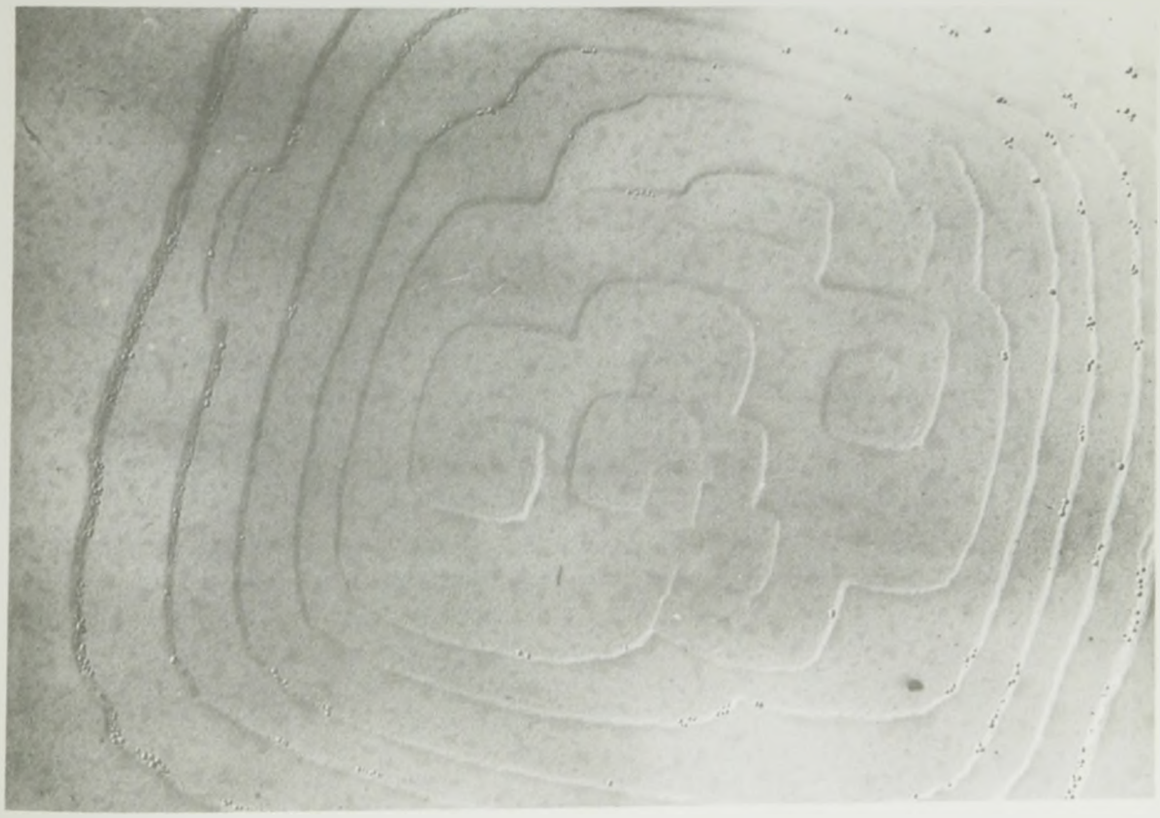

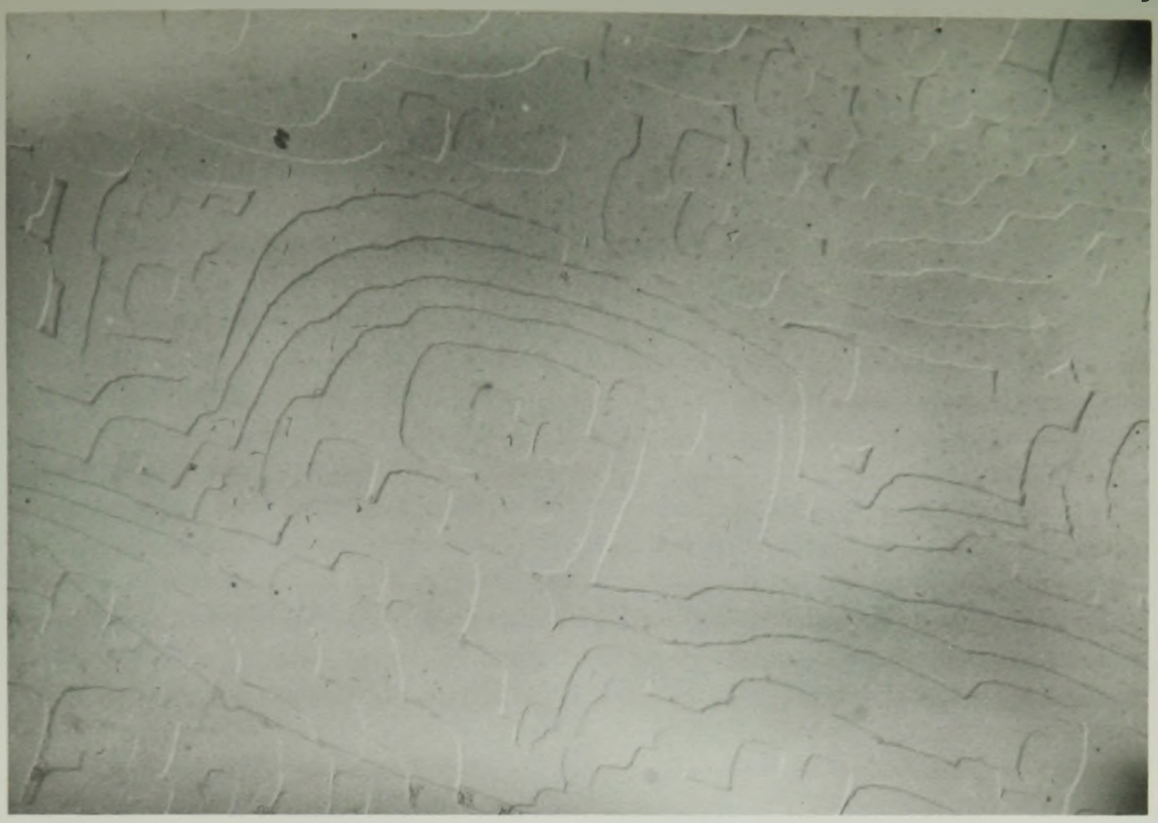

FIGURE 41: Inhibitor concentration 6 p.p.m. Fe.
Time of etching 30 seconds (16,000 X)

FIGURE 42: Inhibitor concentration 9 p.p.m. Fe
Time of etching 10 seconds (16,000 X)

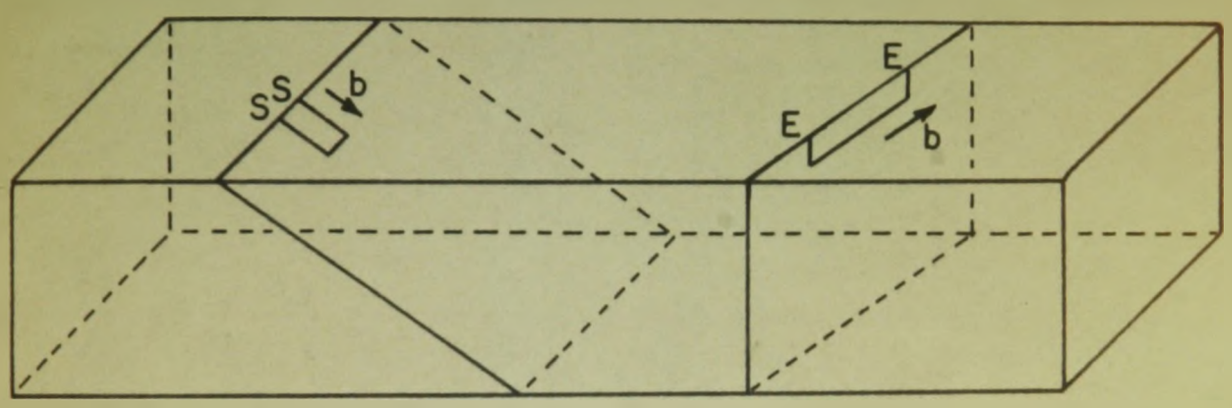

FIGURE 43: Schematic drawing of two dislocation loops that intersect the surface of a cleaved crystal. Screw components emerge at points S, and edge components emerge at points E. Cleavage plane $\{100\}$; Glide plane $\{110\}$; glide direction $\langle 110 \rangle$.

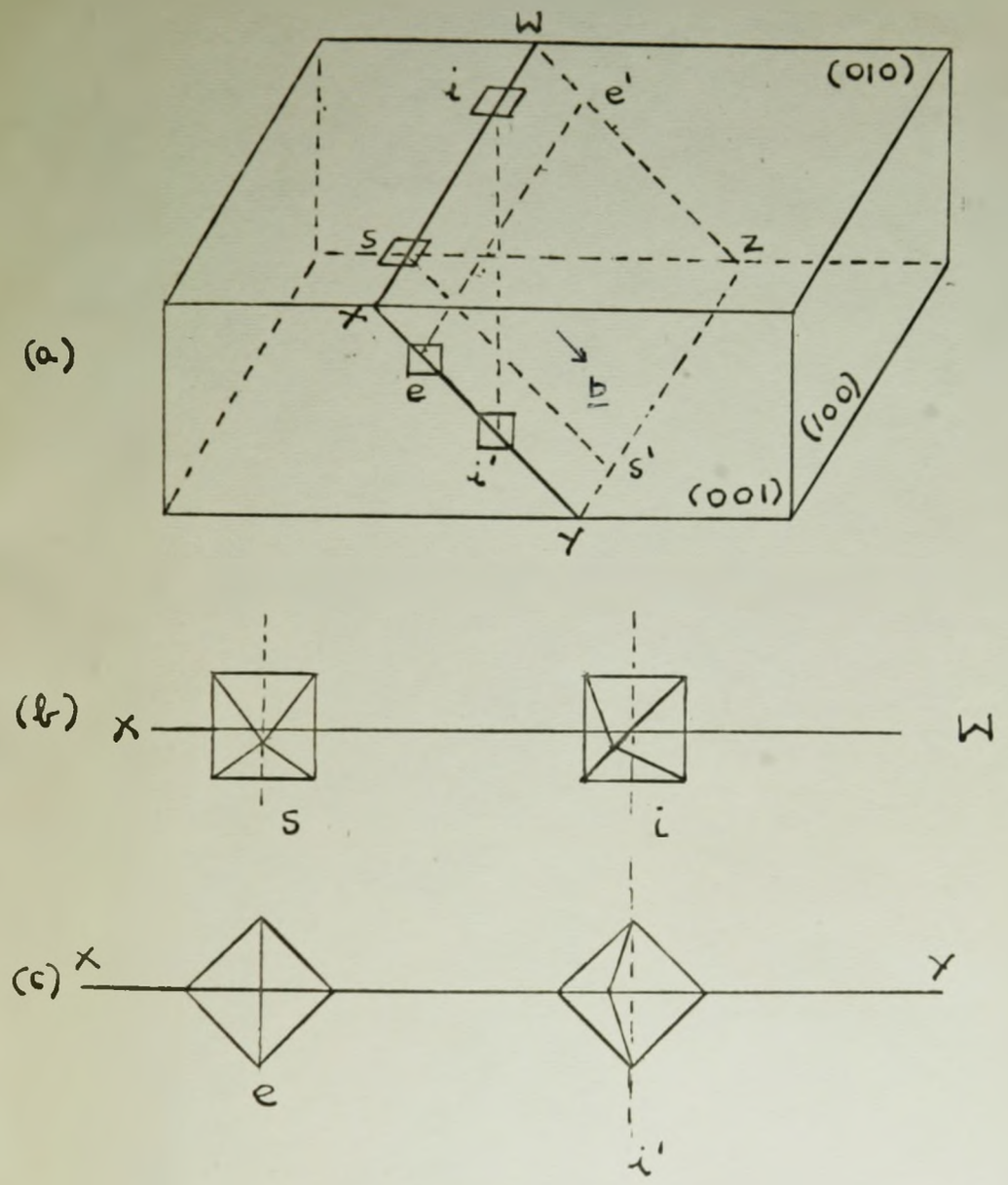

FIGURE 44: (a) Drawing of a cleaved LiF crystal showing the (110) glide plane, marked WXYZ, and the $[1\bar{1}0]$ Burgers vector, b. In the glide plane are shown an edge dislocation, ee', a screw dislocation, ss', and a dislocation of intermediate character, ii'.

(b) Two dislocation pits on glide band XW. The pit on the left corresponds to the pure screw dislocation, and the pit on the right corresponds to the intermediate dislocation.

(c) Two dislocation etch pits on glide band XY. The pit on the left corresponds to the pure edge dislocation, and the one on the right corresponds to the intermediate dislocation.

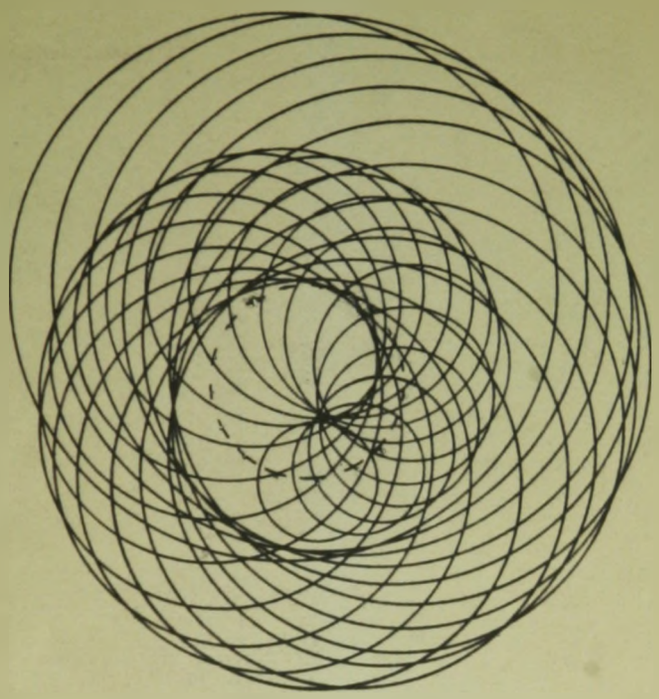

FIGURE 45: Formation of a spiral by dissolution at a helical dislocation.